Geomorphology 370 (2020) 107370

Contents lists available at ScienceDirect

Geomorphology

journal homepage: www.elsevier.com/locate/geomorph

LiDAR-derived high-resolution palaeo-DEM construction workflow and application to the early medieval Lower Rhine valley and upper delta

B. van der Meulen [a,*], K.M. Cohen [a], H.J. Pierik [a], J.J. Zinsmeister [a,b], H. Middelkoop [a]

[a] Department of Physical Geography, Utrecht University, Princetonlaan 8a, 3584 CB Utrecht, the Netherlands
[b] Division of Geography and Tourism, KU Leuven, Celestijnenlaan 200e, 3001 Leuven, Belgium

ARTICLE INFO

Article history:
Received 28 August 2019
Received in revised form 4 August 2020
Accepted 4 August 2020
Available online 6 August 2020

Keywords:
Palaeo-DEM construction
Palaeotopography
Rhine
Floodplain

ABSTRACT

Reconstruction of past topography in palaeo-DEMs serves various geomorphological analyses. Constructing a palaeo-DEM by stripping young elements from a LiDAR DEM can provide results for large study areas at high resolution. However, such a 'top-down' approach is more suited to recent periods and geomorphologically static parts of the landscape than to geomorphologically dynamic areas and periods farther back in time. Here, we explore this approach by reconstructing the early medieval (circa 800 CE) topography of the Lower Rhine river valley and upper delta in Germany and the Netherlands. The large (4500 km^2) study area contains abundant anthropogenic terrain modification and stretches across geomorphologically active as well as inactive zones. We first removed all anthropogenic relief elements from the LiDAR DEM, using separate procedures for linear and non-linear elements. These steps were sufficient to obtain the palaeotopography of the inactive zone, characterized by inherited natural relief. Then, we reconstructed the topography and bathymetry in the fluvially-reworked active zone by incorporating geological and historical geographical information. We present and evaluate zonal averages of elevation differences between the modern and past valley floor topography in this densely populated area with complex land-use history, which allows us to approximate total anthropogenic volumetric change. Further comparisons with the modern LiDAR DEM elucidate changes in floodplain negative-relief connectivity, showing the potential importance of investing in palaeo-DEMs when assessing past river flooding. Our palaeo-DEM construction workflow is deployable at diverse spatial scales and widely applicable to other lowland areas, because of its top-down and generic nature. The relative importance of different workflow aspects depends on the time period that is targeted. Beyond a target age of 10–15 ka, valley floors that are too large in area are to be considered geomorphologically dynamic and the top-down approach to palaeo-DEM construction is no longer advisable.

1. Introduction

The geomorphology of many parts of the world has been altered by humans (Tarolli and Sofia, 2016; Brown et al., 2017). For this reason, a Digital Elevation Model (DEM), even with non-ground points such as buildings and canopies filtered out, for a typical inhabited area does not represent a natural state of the topography. This is especially true for lowland river areas, which often are densely occupied, with long histories of human modifications to the terrain, and lose natural relief quickly because of modest elevation differences (Lewin and Ashworth, 2014). The present topography, altered by human as well as fluvial activity, is not readily applicable in quantitative analyses of past landscapes and landscape processes. Instead, such analyses require a palaeo-DEM that represents the topography of a historical or natural situation.

The need for palaeo-DEMs is widespread across geomorphological studies focusing on reconstruction or modelling, on both short (<10^3 yr) and longer (>10^3 yr) time scales, and at a variety of spatial scales. At a regional scale, palaeo-DEMs help to understand the historical and geomorphological evolution of an area (Werbrouck et al., 2011; Vermeer et al., 2014; Pierik et al., 2017; Briant et al., 2018; Pierik and van Lanen, 2019), and aid in landscape-archaeological regional inventories and archaeological modelling (Cohen et al., 2017; van Lanen et al., 2018; van Lanen and Pierik, 2019). At a local scale, palaeo-DEMs are key to identify past natural and artificial drainage network elements (Baubiniene et al., 2015; Kirchner et al., 2017; Schmidt et al., 2018), and to map the geomorphological contexts of early settlements and urban centres (Schneider et al., 2017; Mozzi et al., 2018; Grimm and Heinrich, 2019; Pröschel and Lehmkuhl, 2019). Further, lowland palaeo-DEMs are essential in numerical simulations of past extreme flood events such as tsunamis (Röbke et al., 2016; Wronna et al., 2017) and large river floods (Hesselink et al., 2003), although recent river-flood palaeohydrological research so far has relied on one-

* Corresponding author.
E-mail address: b.vandermeulen@uu.nl (B. van der Meulen).

https://doi.org/10.1016/j.geomorph.2020.107370

dimensional cross-sectional analyses (Herget and Meurs, 2010; Toonen et al., 2013; Herget et al., 2014; Benito and Díez-Herrero, 2015).

Two contrasting approaches exist for constructing a palaeo-DEM (Fig. 1). The first is to reconstruct the past terrain 'bottom-up' from interpolating spotty observations on sedimentary surfaces derived from geological, pedological, and archaeological data (e.g., Kirchner et al., 2017). The second is to reconstruct the past terrain 'top-down' from a modern DEM, stripping young relief elements to obtain the past topography, keeping the parts of the DEM that have remained unchanged and interpolating voids (e.g., Schmidt et al., 2018). Often, a combination is used (e.g., Pierik et al., 2017). The bottom-up approach demands specific data, such as sedimentary profiles with good age constraints, and is sensitive to differences in observation density and quality across the study area. It is primarily useful for relatively small (<1 to 10s km^2) areas where sufficient data are available to achieve the resolution and accuracy required for the palaeo-DEM application in mind. A key benefit of the top-down approach is that the required data are often regionally collected and publicly available, both the LiDAR input DEM and digital datasets of infrastructure and land use with 'to strip' features. For this reason, the top-down approach is the more suitable method for reconstructions of larger areas (>10s km^2). Only a few studies provide a generic workflow to construct palaeo-DEMs (Werbrouck et al., 2011; Vermeer et al., 2014; Pierik et al., 2017; Schmidt et al., 2018) and, so far, limits and trade-offs in terms of resolution and temporal reach of different approaches have not been evaluated.

The aim of our study was to develop a workflow for palaeo-DEM construction and apply this to reconstruct the early historic topography (target age: circa 800 CE) along the Lower Rhine at high spatial resolution (50 × 50 m) to be useful in mapping and modelling applications in fluvial geomorphology and palaeohydrology. The target age of the palaeo-DEM shortly predates the onset of river dike construction in the Rhine delta. Because river dikes were the first major anthropogenic relief elements in the study area, the period around 800 CE represents a last semi-natural state of the river and floodplain without direct human modifications. This implies that constructing a valley-wide palaeo-DEM and quantifying elevations differences with the modern day provides a volumetric quantification of medieval-to-modern net anthropogenic topographic change. Presenting results on this was a secondary aim of the study, also because it is a way to evaluate the quality of the palaeo-DEM. Our discussion section evaluates the top-down approach to large-scale valley floor palaeo-DEM construction for younger historic and older prehistoric periods.

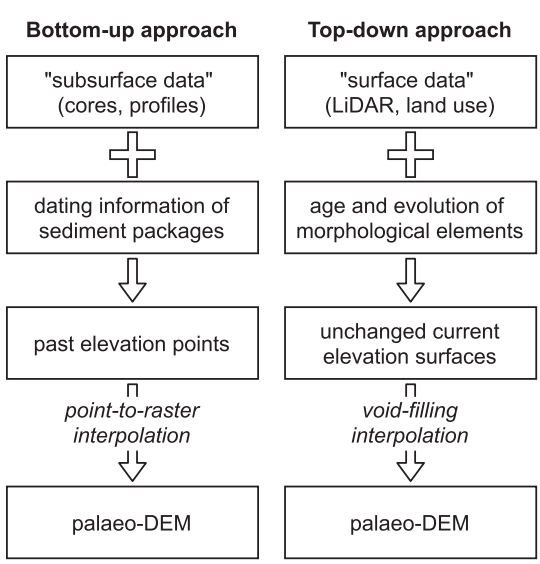

Fig. 1. Workflow outlines for two main takes on palaeo-DEM construction, contrasting the 'bottom-up' and 'top-down' approaches.

The study area covers the full width of the Lower Rhine valley and upper delta. This large (4500 km^2) lowland region is an excellent case for exploring and evaluating large-area high-resolution palaeo-DEM construction, because (1) there are many anthropogenic modifications to the terrain, (2) there are geomorphologically dissimilar zones, with and without fluvial activity since the time period represented by the palaeo-DEM, and (3) abundant data are available from multiple disciplines on for example floodplain ages (e.g., Klostermann, 1992; Erkens et al., 2011; Cohen et al., 2012) and past river positions (e.g., Hoppe, 1970).

We describe the workflow for palaeo-DEM construction in detail, highlighting the generic aspects of each step. The workflow is a dominantly top-down approach, based on LiDAR DEM adaption rather than geological methods. The most important steps concern stripping anthropogenic features from the LiDAR DEM. In addition, we account for natural processes that affect the topography, after distinguishing the zone within which, in historic times, the Rhine laterally migrated and cut off meander bends. Our workflow, consisting of both automated and manual steps, is applicable to lowland settings at different spatial scales and resolutions. We first show how we applied the workflow to the Lower Rhine study area. Then, we analyse the resulting palaeo-DEM on aspects relating to human and fluvial activity as well as the role of the floodplain in the fluvial system. Next, we evaluate the workflow and the implications of our choices on the accuracy of the palaeo-DEM. We end with a discussion of the wider applicability of the workflow and provide a detailed framework for adjusting the workflow to different, earlier or later, time periods.

2. Study area

The study area of 4500 km^2 covers the Lower Rhine valley and upper delta in Germany and the Netherlands (Fig. 2). The area has been a strategic corridor and barrier for many millennia. It functioned as the border for the Roman Empire between 50 BCE and 450 CE, and again in stages of the Carolingian German empire and on and off in all historic periods since including WWII (e.g., Begbie and Roberts, 2014). The crossings of the 'barrier' of the Rhine by warring parties, whether for the purpose of military conquest or retaliation, are repeatedly mentioned in historical accounts ever since the Gallic wars of Julius Caesar around 50 BCE (e.g., Breeze et al., 2018), and part of the narrative of the Unesco heritage status nomination (FRE-LGL, 2019) for the linear scatter of first to third cy CE Roman military border infrastructure archaeological legacy on the left side of the then Rhine. The Rhine valley was a transportation corridor to humans in prehistory and history alike. Neolithic agriculture and the tribes that introduced it spread into the study area along the Lower Rhine (Louwe Kooijmans, 2007; Denis et al., 2019). Roman-age military patrolling roads and forts guarded the Rhine as a shipping route (FRE-LGL, 2019 and abundant sources therein). Early and high medieval land and river trade (notably at Duisburg; Krause, 1997, 1999, 2003) continued to use these river routes (e.g., van Lanen et al., 2016). Medieval tolling privileges were manifold, e.g., fourteenth cy Guelders Lobith/Tolkamer and Cleves Griethausen at the later Dutch-German boundary (Overmars, 2020), when river trade became managed by the Hanseatic league.

The population density of the study area is high and the land use in the Lower Rhine valley and upper delta plain today is a complex patchwork characterized by industry, intensive farming, and dense urbanization. Consequently, the area features abundant anthropogenic modifications to the pre-industrial topography and original natural geomorphology of the valley floor (active and abandoned meandering channels, variable floodplain topography, flood-free terraces). Positive anthropogenic relief is formed by dikes, embankments for highways and railroads, mining and waste dump sites, and other raised grounds. Negative anthropogenic relief is formed by clay and gravel quarries and pits, harbours, and other dug features. Particular forms of human-induced negative relief area are coal mining-related subsidence bowls

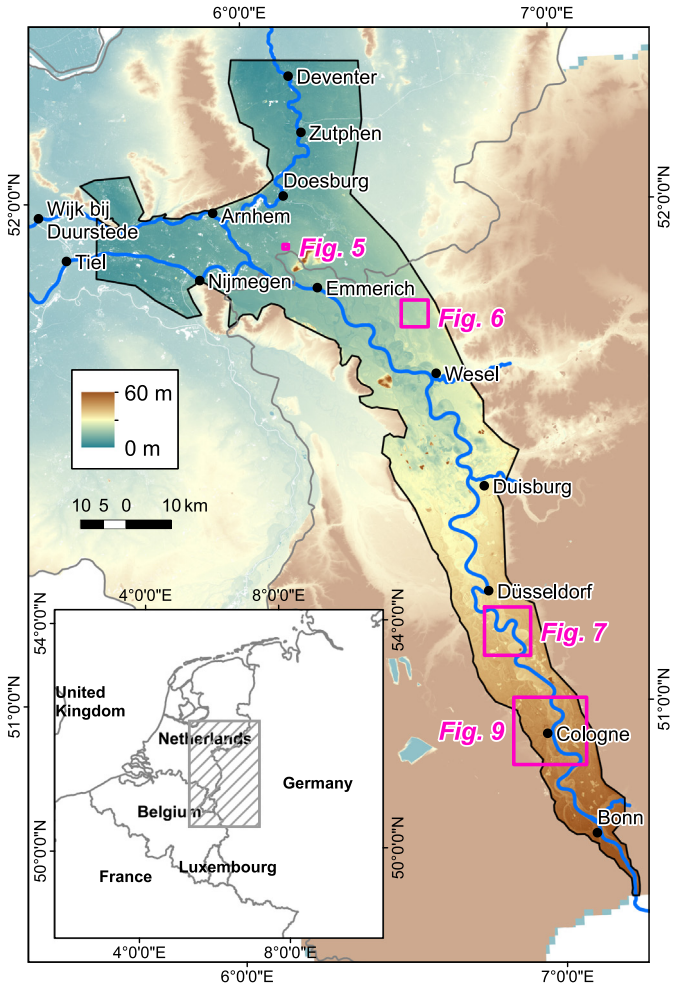

Fig. 2. Extent of the study area covering 4500 km^2 in North Rhine-Westphalia (Germany) and the Netherlands. Background is the LiDAR DEM data (DGM1-BrK, 2017; AHN2-RWS, 2013) as merged for the two countries (see text for resolution information: 1 × 1 m as original download; 5 × 5 m in our 'stripping' processing; coarser in post-processing and foreseen usage).

that developed during the twentieth century (e.g., Harnischmacher and Zepp, 2014).

The axial zone of the study area is occupied by the Lower Rhine, which was a freely meandering river up to historic times, when it became increasingly human-modified. In the nineteenth century, extensive river training measures were carried out that confined the flow and halted lateral migration along the entire river course (Kalweit et al., 1993). In the north of the study area, close to the German-Dutch border, the Lower Rhine valley floodplain grades into the Rhine delta plain (Klostermann, 1992; Erkens et al., 2011). Here, the Lower Rhine bifurcates into the distributaries Waal and Nederrijn (Fig. 2). The history of the delta apex is well known from earlier geological, sedimentological, and historical work, including studies focusing on past oscillations in channel sizes and related discharge division (van de Ven, 1976; Kleinhans et al., 2011). At present, the southern distributary of the Rhine (the Waal) is the largest, but in medieval times the northern distributary (the Nederrijn, Dutch for lower Rhine) was the largest. Discharge partitioning between the branches Waal (66%) and Nederrijn (33%) today is 2:1 and engineering controlled. Partitioning before 1500 CE was in favour of the Nederrijn (>50%; e.g., Kleinhans et al., 2011), indicated by first millennium CE meander morphologies, geoarchaeological findings and classic historical accounts (e.g., Verhagen et al., 2017). Near the city of Arnhem, a second bifurcation results in the Gelderse IJssel distributary (Fig. 2). This northward river branch began avulsing between 600 and 800 CE and reached a full size between 1100 and 1500 CE (Makaske et al., 2008; Groothedde, 2010; Cohen et al., 2012).

The upstream boundary of the study area is placed 15 km upstream of the city of Bonn, where the Rhine river leaves the bedrock-confined zone of the Middle Rhine and enters the alluvial reaches of the Lower Rhine valley (Klostermann, 1992; Erkens et al., 2011). The downstream boundaries are placed at the transition of the upper delta plain to the lower delta plain, where river flow and water levels come within reach of tidal influence (e.g., Berendsen and Stouthamer, 2001; Gouw and Erkens, 2007). The lateral boundaries of the study area are placed at the flanks of Middle Pleistocene (Saalian) landforms. In the upstream part of the study area, these are the lowest middle terraces (cf. Klostermann, 1992); in the downstream part, these are ice-pushed ridges and glacio-fluvial outwash landforms. The lateral boundaries define a maximum floodplain extent that, from the river channel outwards, includes the modern floodplain, all former Holocene floodplains and channels, and the surfaces of Late Pleistocene terraces (Fig. 2).

3. Materials

We here declare the various materials (listed in Table 1; located in Fig. 3) incorporated and otherwise made use of in the palaeo-DEM construction workflow. This started with airborne LiDAR data of North Rhine-Westphalia (DGM1-BrK, available as open data since 2017) and the Netherlands (AHN2-RWS, available as open data since 2013) – currently standard LiDAR data products in which buildings and vegetation

Table 1
References of materials used. Spatial extents are indicated in Fig. 3.

A. Geology and geomorphology		B. Archaeology and historical geography	
No.	Reference	No.	Reference
1	DGM1-BrK, 2017	21	Schneider, 1886
2	AHN2-RWS, 2013	22	Höltken and Wagner, 2015
3	Klostermann, 1992; Erkens et al., 2011	23	Straßer, 1989
4	Zhou, 2000	24	Gerlach, 2006
5	Shala, 2001	25	Scheller, 1965
6	Toonen, 2013	26	Hoppe, 1970
7	Klostermann, 1986	27	Harnischmacher and Zepp, 2010, 2014
8	Heine and Siebertz, 1980	28	Scheller, 1957; Krause, 1997, 1999, 2003; Meurers-Balke et al., 1999
9	Berendsen and Stouthamer, 2001	29	Bechert, 2007
10	Koomen and Maas, 2004	30	Gerlach, 2003
11	Cohen et al., 2012	31	Cohen et al., 2014
12	Cohen et al., 2017	32	Heunks and van Hemmen, 2016; Willemse, 2019
13	Kleinhans et al., 2011		
14	Pierik et al., 2017		

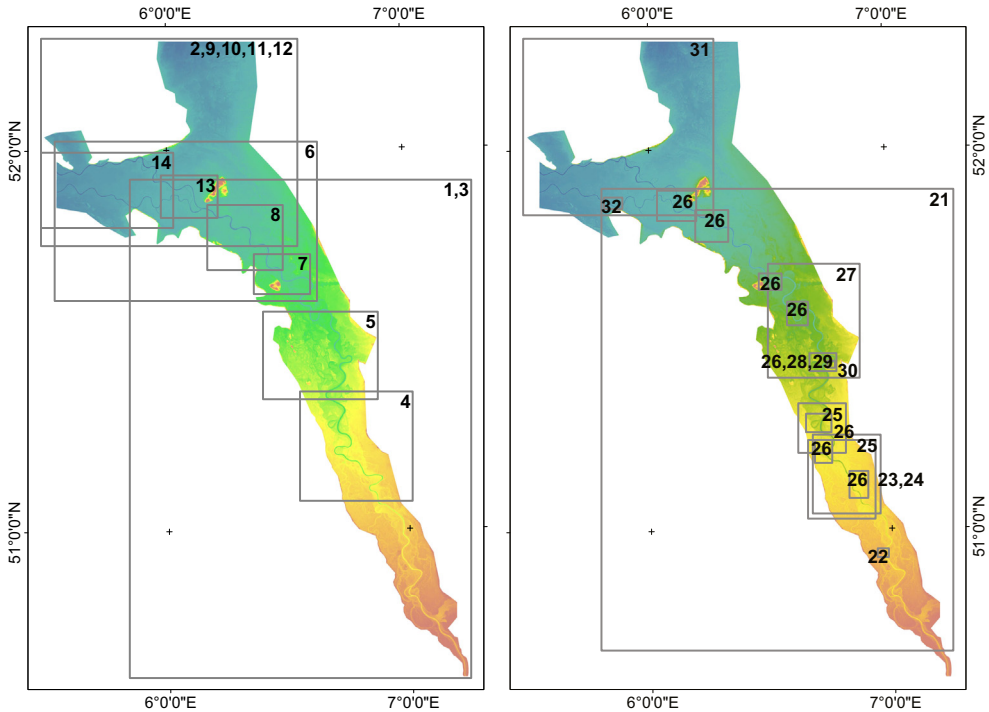

Fig. 3. Overview of materials used, with their spatial extents indicated by rectangles on the study area (as in Fig. 1). Left panel shows geological-geomorphological information sources (numbered 1–14; referenced in Table 1); right panel shows archaeological and historical sources (numbered 21–32; referenced in Table 1). Not indicated are starting-point resources covering the complete study area (OpenStreetMap vector data, RWS-LANUV Baseline bathymetric data, satellite imagery).

have been filtered and removed so that grid-cell values represent the ground surface. Together, this provided land surface elevations over the full study area (Fig. 2). Survey data on the bathymetry of the river bed were obtained from river managing authorities (part of the RWS-LANUV Baseline dataset). A dataset quantifying elevation changes in the Ruhr area was obtained from the study of Harnischmacher and Zepp (2010, 2014), who quantified positive and negative elevation change between historical survey data from nineteenth century topographic maps and present-day elevations. The six western-most map sheet tiles of their dataset overlap with our study area, and for this subarea we isolated underground mining-induced depressions in order to correct for this subsidence. We note that relatively accurate results were obtained for this subarea of near-horizontal valley floor (regional gradient = 0.2–0.3 m/km; e.g., Erkens et al., 2011; Toonen et al., 2013), where the error associated with nineteenth-cy contour mapping is regarded ≪1 m (Harnischmacher and Zepp, 2014; their Fig. 3). The above datasets, with some merging, resampling and warping operations (see Section 4.1) allowed us to prepare an 'Input DEM' at 5 × 5 m processing resolution (Fig. 4).

Next, to supply the series of workflow steps that strip anthropogenic features from the LiDAR data, we incorporated land-use datasets that identify such elements. We mainly used OpenStreetMap, since this dataset is in vector format and one of the few high-resolution datasets that covers more than a single country, and uses nearly consistent feature attributes across nation boundaries. Initial tests and visual inspections confirmed that for the type of features targeted within the dataset (see Table 2), this volunteer-generated open dataset is accurate in our study area. River dike positions in vector format were supplied from the previously mentioned Baseline dataset that provides these in a consistent format at both sides of the border, and supplemented with dike elements from the digital geomorphological map of the Netherlands (Koomen and Maas, 2004). As additional visual reference, we used satellite and aerial imagery for identification of anthropogenic landforms.

Next, we incorporated data from different disciplines providing information on the development of the Rhine river (Fig. 3; Table 1). These allowed to identify the zone within which the river has migrated in the last 500 yr (historic maps), 500–1000 yr (medieval settlements and written descriptions including position and dates for bend cut-offs), 1000–1500 yr (geoarchaeology, scarce older descriptions, some radiocarbon dating), 1500–2000 yr (archaeology, few classic roman texts, some radiocarbon dating), and so on (some archaeology, mostly geomorphology, pedology and quaternary geology). This constrained and informed the palaeo-DEM construction workflow for the active zone: the part of the study area where the landscape has been reworked by natural processes (besides human activity) since the target age. Given the extent of the study area, the developed state of prior research, and the volumes of potential raw data to be used - rather than taking in primary observational data (individual point observations collected by field geologists, soil mappers, archaeological excavators, archive visiting historians), earlier compiled map datasets were used as the starting point. Klostermann (1992) and Cohen et al. (2012) provide referenced ages for individual meanders with superregional coverage. These allowed us to digitally select the active meandering zone for a given time period to demarcate the active zone, which is a requirement for meaningful palaeo-DEM construction. Geological-geomorphological studies of subregional coverage provided further detail (references 4–8 in Table 1). Most datasets were created before LiDAR DEM data became available for the German part of the study area. This meant that using them to demarcate our active zone required some re-digitizing to improve the accuracy of digital mapping of floodplain-edge scarps.

Within the active zone, by definition and implication, direct superficial geomorphological features allowing us to pinpoint river channel positions in early historic times are lost to younger reworking. Still, historical, historical geographical, and archaeological studies (references 21–32 in Table 1) give sufficient information to address past positions of the Rhine channel, either by inference from archaeological data, or by interpretation from historic written information (e.g., first settled ages, settlement abandonment dates, meander cut-off years and locations).

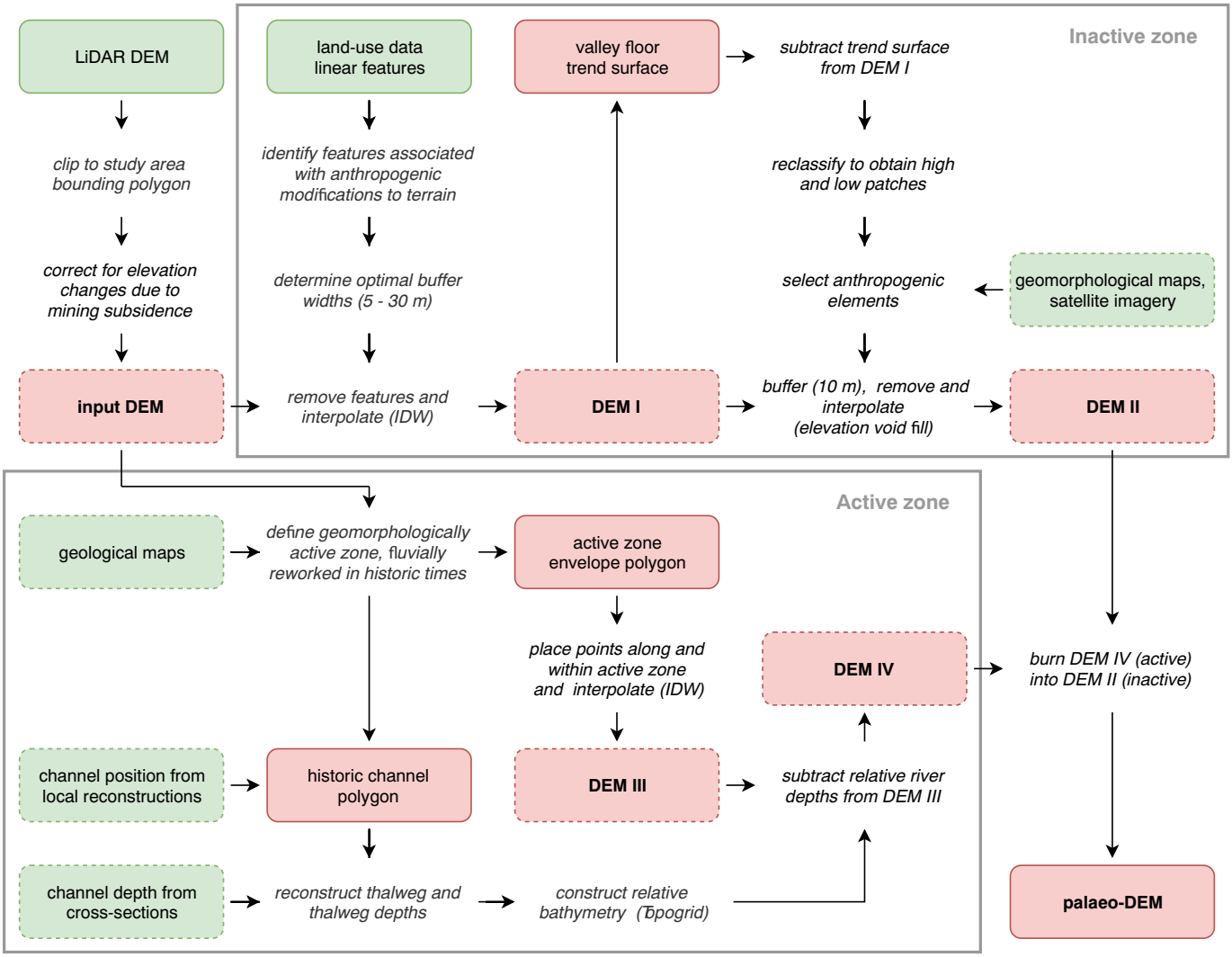

Fig. 4. Workflow for large-scale valley-floor palaeo-DEM construction using a dominantly top-down approach. The upper part of the workflow depicts steps for a geomorphologically inactive zone carrying anthropogenic overprints and the lower part depicts additional steps for an active zone with younger-than-target age river meandering besides anthropogenic overprints. Data products in coloured boxes, operations in italics. Input in green, with dashed borders indicating non-essential input used indirectly as guidance. Output in red, with dashed borders indicating intermediate output.

4. Methods

4.1. Preparing the Input DEM

As first steps, preceding palaeo-DEM construction, we merged the LiDAR data (AHN2: 0.5 × 0.5 m resolution in the Netherlands National Grid; DGM1: 1 × 1 m resolution resampled from the German to the Netherlands Grid) and inserted the RWS-LANUV Baseline channel bathymetry. We then clipped this assemblage to the study area. One subregion within our study area is known to be affected by underground mining-caused subsidence, so we pre-treated the LiDAR DEM for this subarea before starting the generic workflow deployed along the entire valley. We obtained the grid of elevation differences between nineteenth cy maps and modern elevation from the Harnischmacher and Zepp (2010) study, selected all grid cells with negative elevation change and made further masking deselections (harbour canal linear elements, surficial aggregate mining) to arrive at a final selection that isolated bowl-shaped depressions in areas with otherwise natural paleochannel relief (e.g., on map sheet Rheinberg 4405: 1–2 km in diameter, up to 6 m subsidence in the centre, near zero at the edge) in the LiDAR DEM for recent (twentieth cy) mining-induced subsidence. We deployed void-fill techniques to interpolate the subsidence patterns in deselected areas. We then applied a low-pass smoothing filter and used the result as a warping grid to bring depressed areas in the merged LiDAR+bathymetry DEM to a representative present elevation. This provided the 'Input DEM' used as starting point of our palaeo-DEM construction workflow (Fig. 4), at a resolution of 5 × 5 m.

Table 2
Buffer widths for anthropogenic linear elements used in DEM stripping.

Feature	Source	Buffer (Germany)	Buffer (Netherlands)
Highway	OpenStreetMap	30 m	30 m
Trunk road	OpenStreetMap	20 m	20 m
Primary road	OpenStreetMap	25 m	25 m
Secondary road	OpenStreetMap	20 m	10 m
Tertiary road	OpenStreetMap	5 m	5 m
Railway	OpenStreetMap	30 m	30 m
Bandijken (main river dikes)	RWS-LANUV Baseline	–	30 m
Kades (artificial levees)	RWS-LANUV Baseline	30 m	–
Hoge dijk (high dike)	Alterra GKN	–	15 m
Middelhoge dijk (medium high dike)	Alterra GKN	–	15 m
Lage dijk (low dike)	Alterra GKN	–	15 m

The reasons to resample the merged LiDAR data and mining-subsidence grid to 5 × 5 m cell size for the Input DEM (above) and the further

processing (next sections) were: (i) lower accuracy demands on the vector datasets used to mask, remove and re-interpolate anthropogenic features, and to demarcate the riverine active zone (young meanders) from the inactive floodplain and older valley-floor landforms (older meanders, flood-free terraces), and (ii) lower digital data storage and computational processing time for the relatively large study area (4500 km^2 at 5×5 m equals $180 * 10^6$ raster cells).

4.2. Demarcating the inactive and active zones

A key step in the workflow is to distinguish a geomorphologically inactive distal floodplain zone and a geomorphologically active fluvially-reworked zone. To demarcate this zone, the workflow requires a decision on the palaeo-DEM target age. The steps that follow reveal that for stripping anthropogenic features we do not use further specific age information (Section 4.3), whereas for positioning the target-age river channel in the active zone we do (Section 4.4).

In the inactive zone, by definition and implication, the terrain surface is defined by anthropogenic topographic signatures superimposed on the relief inherited from times before the palaeo-DEM target age. In our valley-floor setting, quasi-natural processes such as superficial net erosion on tilled fields and net sedimentation owing to occasional larger floods (when embankments were overtopped) are very modest over most of the very gently sloping valley floor and upper delta plain (hence the label 'inactive'), and vertically much smaller than the aforementioned anthropogenic overprints that we target to remove. The active zone, on the other hand, is characterized by abundant natural and quasi-natural geomorphic processes that have continued to alter the relief in more recent times. Here, the natural terrain surface has been shaped by erosion and sedimentation processes since the target age (800 CE). Human influence has also played a major role in modifying the terrain in the active zone, but recent fluvial activity dominates. Creating a palaeo-DEM for the active zone thus requires additional reconstruction steps compared to the inactive zone, where stripping all anthropogenic elements from the LiDAR DEM provides a good representation of the early historic geomorphology. For the inactive zone, the earlier introduced 'top-down' stripping methods are sufficient to transform the Input DEM starting point to the palaeo-DEM end product (Fig. 4: upper part), whereas for the active zone, an additional method allowing for restoration is needed (Fig. 4: lower part).

Our way to demarcate the active from the inactive zone was to make use of existing geological mapping datasets (references 3 and 11 in Table 1; polygon vector GIS), and query these digitally to return the areas considered geologically younger than the target age for the palaeo-DEM. In this way, we aimed to select a ribbon-shaped polygon representing the post-800 CE channel belt of the Rhine, i.e., the zone of meander migration activity since 800 CE. Regarding the dating accuracy of the existing geological mapping products: superregional overview maps of the area typically identify a Late Holocene channel belt (e.g., Klostermann, 1992; Erkens et al., 2011), and regional and local geological and historical mapping (e.g., various sources in Table 1) then provides abandonment ages for individual meanders within based on radiocarbon dating, historic sources, and cross-cutting relationships.

Dating accuracy for individual meanders varies. For Rhine meanders from the common era, it is quite good, owing to archaeological attention to the Roman occupation period (50 BCE to 450 CE) of the left bank of the Lower Rhine. It is 'to the year' in the best cases (going back to the fourteenth century CE), to ± 100 years in most cases, and to ± 200 years in the poorest age-control cases. This is the dating accuracy of fragmentary abandoned meanders (start of infilling of oxbow lakes), which controls the spatial accuracy at which one can pinpoint the contemporary floodplain edge and the river channel position in the target age situation. To assess mapping spatial accuracy, the map boundaries of geologically-dated meanders that provided our initial delimiting of the active zone were confronted with the LiDAR imagery. This revealed feature-boundary mapping inaccuracies locally exceeding 50 m where data products had been created prior to LiDAR availability. Hence, we updated the initial zone polygon outline to have it match morphological scarps more closely (within 5 m). Where anthropogenic landforms overlie scarps marking the active zone, the active zone was enlarged to fully include the anthropogenic form.

4.3. DEM stripping

For DEM stripping, we deployed a two-step method to remove all anthropogenic elements larger than 50 m as well as most smaller elements. The first step, leading to DEM I (Fig. 4), involved land-use data. From these, we selected linear features associated with significant anthropogenic modifications to the terrain (for example, major roads and railroads), which in our study area are commonly built on embankments (Fig. 5A). Then, we placed buffers around the selected elements defining the width of terrain modification (Table 2). Buffer widths were chosen large enough to fully mask out the sloping sides of features, but at the same time were kept as small as possible to minimise introduction of interpolation artefacts. Determining buffer widths therefore required some scrutiny and varied per feature type. In the buffer zones (white area in Fig. 5B), we replaced LiDAR-derived elevations with interpolated values, applying Inverse Distance Weighting (IDW, power 2) as a simple and fast interpolation method, applicable to filling smaller voids (e.g., Reuter et al., 2007). The IDW interpolation used abundant remaining LiDAR elevation data surrounding the linear buffer zones. This abundance of data and the relatively small removal buffer widths explain the good results produced (Fig. 5C).

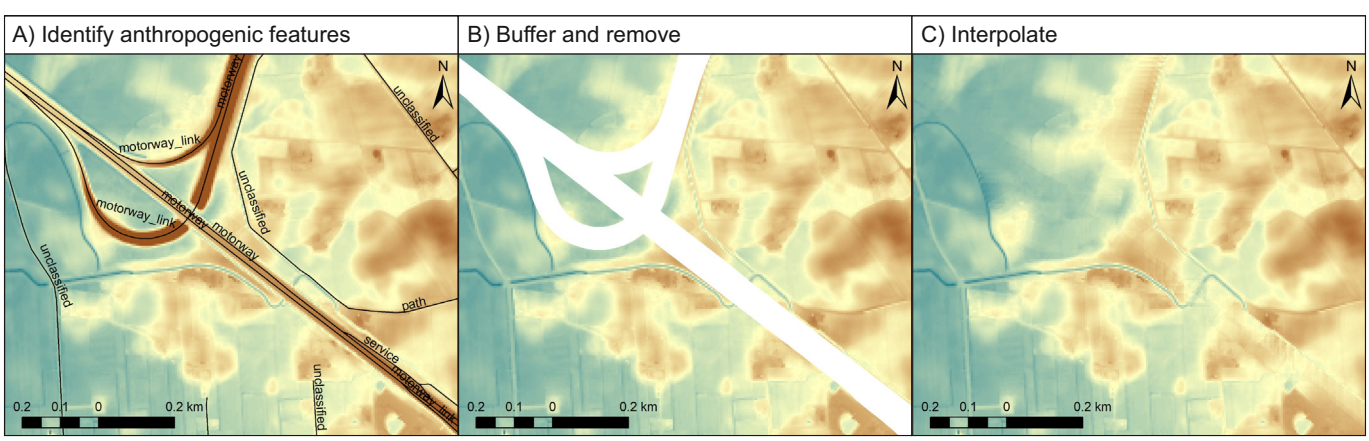

Fig. 5. Automated removal of highway-related elevated grounds from the LiDAR DEM. Panel A shows infrastructure vector lines from OpenStreetMap. Panel B shows the applied buffers (Table 2). Panel C shows the final result. Location indicated in Fig. 2.

The second step proceeded from DEM I (Fig. 6B) and targeted removal of remaining anthropogenic relief modifications that are of various types, ages, and dimensions, and mostly non-linear in shape. It is more difficult to select such features from existing high-resolution national-scale datasets, which tend to classify on e.g., usage, rather than on origin (natural versus anthropogenic) or age. Rather than selecting non-linear anthropogenic features based on land-use dataset queries, we manually selected them in a reclassified DEM-of-difference between DEM I and a second-order polynomial trend surface calculated over DEM I (Fig. 6C). In calculating this trend surface, we excluded insular areas of elevated non-floodplain terrain area so that the trend surface represented the average height of the valley floor (Late Pleistocene terrace and younger valley features: the extended Holocene floodplain). In the DEM-of-difference, discrete patches of above- and below-average elevated grounds at vertical intervals of 0.5 m were converted to polygons, and manually classified (geomorphological expert judgement) as 'natural' (to remain) or anthropogenic (to be stripped). Here we compared locations with geomorphological maps and satellite imagery (Fig. 6D), for example to identify quarries and dump sites. Planform morphology of high and low elements was taken into account as part of the judgement. For example, a rectangular-shaped lake in the proximal floodplain is likely the result of quarrying (anthropogenic relief), whereas an irregular curved lake is presumably a natural feature such as a residual channel remnant (natural topography). More generally, steep slopes indicate anthropogenic influence whereas gentle and irregular slopes suggest the presence of natural phenomena. After selecting the anthropogenic elements, we placed buffers around the polygons and removed them (Fig. 6E). A fixed buffer width of 10 m turned out sufficient to remove identified anthropogenic features completely. We interpolated the resulting gaps in the DEM using the elevation void fill function in ArcGIS, filling each gap with a linear surface based on all surrounding cells (Fig. 6F). For relatively large voids, choosing more complex algorithms than IDW generally gives better results (Reuter et al., 2007).

4.4. Reconstruction of topography and bathymetry in the active zone

In what we demarcate as the active zone (Section 4.2), constructing a palaeo-DEM requires the insertion of a restored topography and bathymetry for the target age, which replaces all younger-than-target-age relief (Fig. 7A). To do so, we used the following method that (i) in the end burns in a reconstructed river channel of prescribed thalweg depth, but that (ii) starts off by an active zone void-fill interpolation that makes use of a manually-created set of elevation points (Fig. 7B). The locations of these points were carefully selected (to a total of 6500 points), incorporating geomorphological interpretation of the fluvial landforms to avoid placing points in present and former channels, and favouring areas with remaining alluvial ridge-and-swale relief. We iteratively increased point density (note density variations in Fig. 7B) and visualised preliminary interpolations (IDW, power 0.6) until satisfying results were obtained in the to-be-replaced active zone. This produced a smoothed but otherwise representative palaeo-DEM (DEM III in Fig. 4) for both lower floodplain subareas of the active zone and for terrace rims in places where the river eroded these in historic times (Fig. 7D).

The last steps involved inserting the bathymetry for the separately reconstructed channel position for the palaeo-DEM target age. This

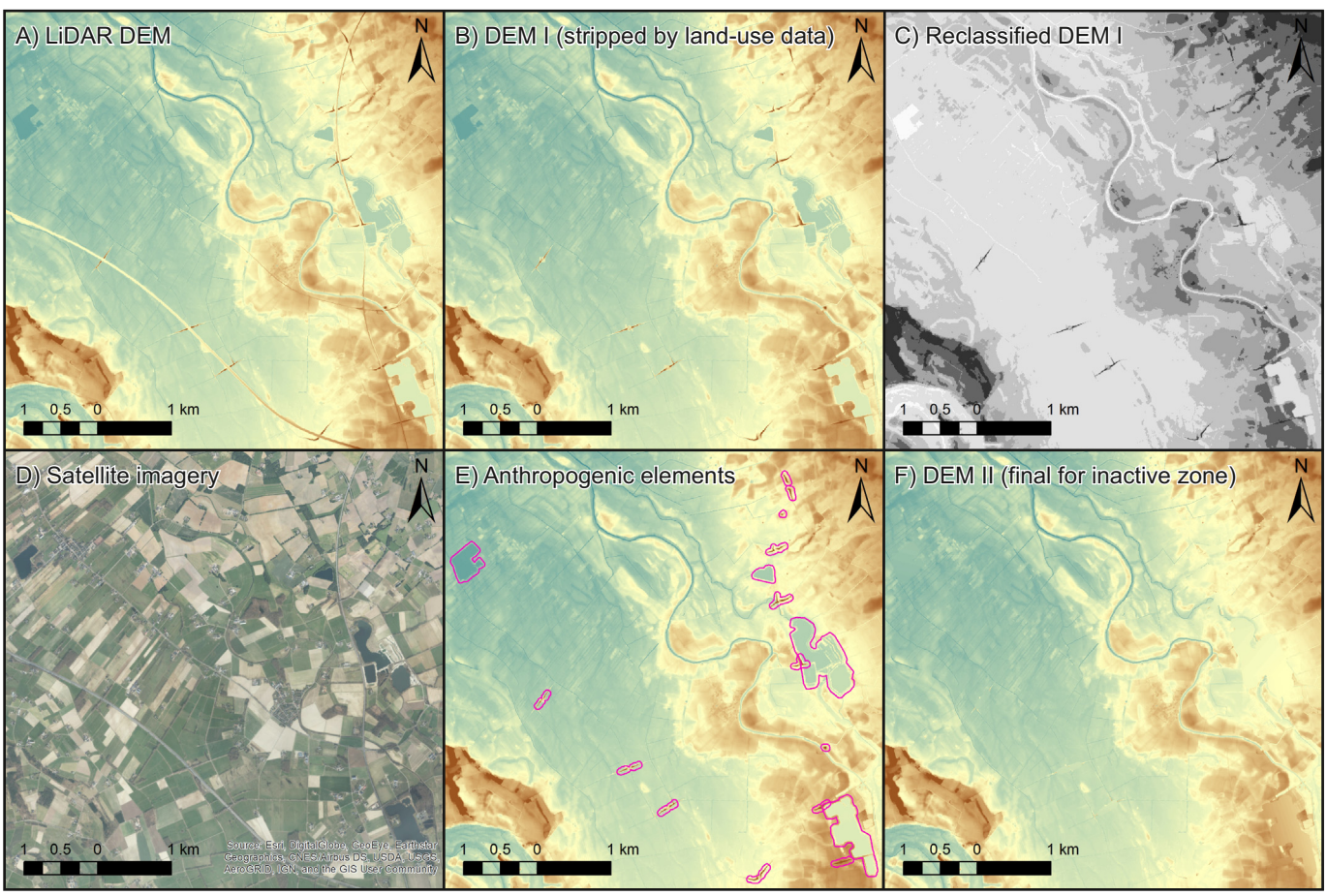

Fig. 6. Removal of diverse anthropogenic elements using a detrended, reclassified DEM. A) LiDAR input DEM. B) Result after stripping linear features such as major roads (DEM I in Fig. 4). C) Detrended, reclassified DEM I (DEM-of-difference between DEM I and a trend surface, see text). D) Satellite and aerial photography reference imagery. E) Polygons selected from the reclassified DEM, manually identified as anthropogenic elements. F) Final result with anthropogenic elements of panel E removed and void-filled (DEM II in Fig. 4). Location indicated in Fig. 2.

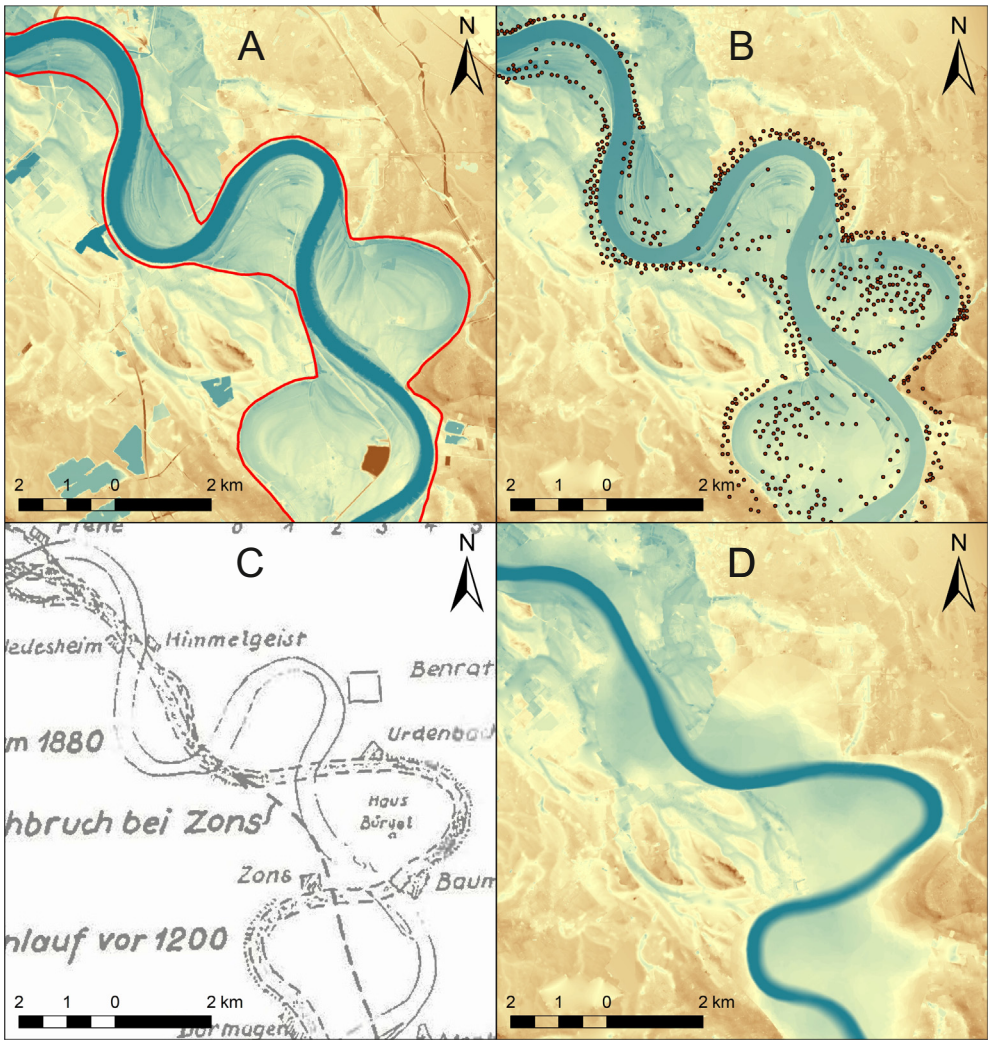

Fig. 7. Reconstruction of floodplain topography in the fluvially-reworked area. A) Input DEM and active zone boundary for meander activity since the target age. B) Intermediate 'stripped' DEM II (still with present river) and manually-placed elevation points along and inside the active zone. C) Example of an earlier reconstruction showing former Rhine river positions (Scheller, 1965), used as input for target-age palaeochannel positioning. D) Final palaeo-DEM for the target age, after interpolating points in B (replacing modern elevation, DEM III) and inserting paleochannel bathymetry from a secondary interpolation (between channel edges and thalweg, DEM IV). Location indicated in Fig. 2.

reconstruction integrated data from various earlier studies in the study area (Fig. 3B), which often provided information at a detailed scale of one to a few meander bends. As Fig. 7C exemplifies, reconstructed channel positions reported in pre-LiDAR studies align well with residual channels and other fluvial geomorphology visible in the palaeo-DEM so far. To decide on palaeochannel widths and thalweg depths, we used geological information (thicknesses of channel fills) as well as historical information (rare in-channel depth measurements on seventeenth–nineteenth cy maps: before modern river engineering, considered young-historic analogues for the river branches in our palaeo-DEM). Existing geological cross-sections (Erkens et al., 2011; Kleinhans et al., 2011; Toonen, 2013) were used to estimate channel depths based on the thicknesses of Late Holocene point bar deposits and channel fills. Over stretches of river in between locations allowing for explicit reconstructions, we assumed similar meander geometries and thalweg depths (i.e., gradual morphological changes).

The thalweg depth values inferred for the target age situation were 8 m, 6 m, and 7 m for respectively the undivided Lower Rhine (Late Holocene representative value), and the deltaic branches Waal (then smaller) and Nederrijn (then larger). We attributed these depth values to thalweg lines, which we positioned close to outer bends inside the reconstructed channel polygons, and interpolated between these lines and the channel edges (depth value = 0 m) using the Topogrid algorithm (Hutchinson, 1993; Topo to Raster tool in ArcGIS). We subtracted these depths from the active zone topography and burned the result into the stripped DEM (Fig. 7D). The active zone of the IJssel branch is treated differently (see Section 4.5), because at the time of the target age this third distributary was not yet a full river (Section 2).

4.5. Post-processing and preparation for method and product evaluations

The methods for inactive and active zone described above aimed to produce a palaeo-DEM for the target age for the Lower Rhine valley and the upper delta (Fig. 8). For that latter area, two earlier palaeo-DEM products were available, at 100 × 100 m resolution. Pierik et al. (2017: main text) using bottom-up methods starting from geological and archaeological borehole and find data had produced a palaeo-DEM for the levee landscape between branches Waal and Nederrijn for 100 CE (representative for the Middle Roman period). Interpolation between the 100 CE and a present surface DEM was used to derive a palaeo-DEM for 900 CE (Pierik et al., 2017: appendices), which we regarded a target equivalent to that of our palaeo-DEM. For along the IJssel river branch, Cohen et al. (2017) provided a palaeo-DEM product for 900 CE derived by combing gridded 3D shallow-geological mapping data products (GeoTOP model) with reconstructions of former natural

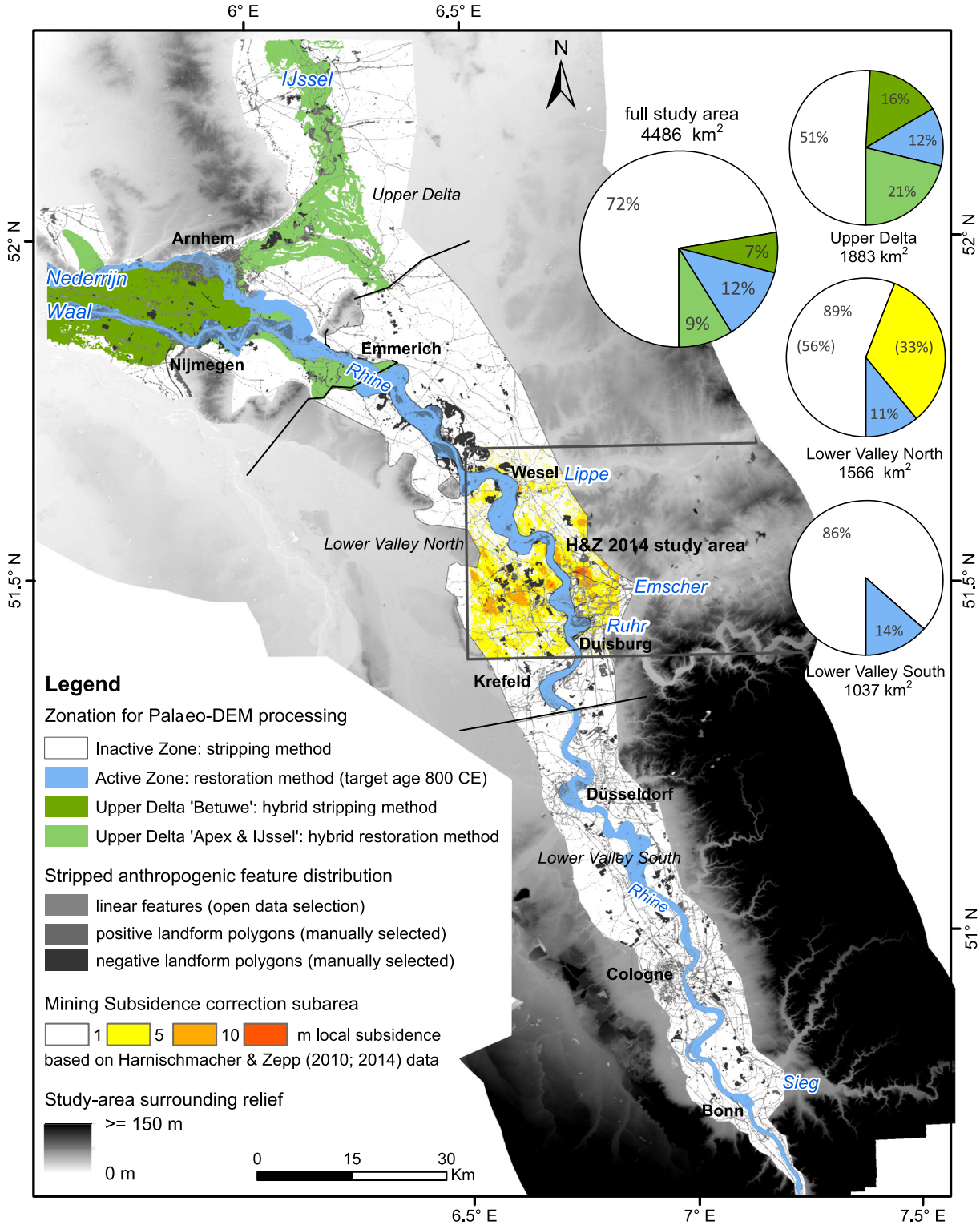

Fig. 8. Evaluation of elevation differences between the present and the palaeo-DEM (executed at 50 × 50 m resolution). Map shows subzones as used in Table 3 and inset charts. Green: upper delta 'central' and 'IJssel' subzones (hybrid methods deployed). Blue: active zone. White: inactive zone. Shades of grey: stripped features. Shades of yellow–orange: subsidence caused by underground mining in area overlapping Harnischmacher and Zepp (2010, 2014) dataset.

deltaic groundwater tables (Cohen, 2005; Koster et al., 2017), featuring a large active zone void (IJssel channel belt; Cohen et al., 2012).

We compared our inactive zone results from the stripping method against these palaeo-DEM produced subregionally using 'bottom-up' methods. Here we resampled the palaeo-DEMs to our production resolution, evaluated elevation difference in the inactive zone, and selected the highest value. The void originating from treating the IJssel branch as an active zone was filled in using the method described in Section 4.4 and Fig. 7B, but without the bathymetry insertion. These solutions for the upper delta 'central' (Pierik et al., 2017) and the 'apex and

Table 3
Regionally-summarized elevation differences between the present and the palaeo-DEM.

Study area division ('zonation')	Surface area		Void-filled subarea		Elevation difference[a]		Cell-based statistics at 50 × 50 m				Volumetric change[a]		Interpretative remarks: attribution
	km²	% total	km²	% subarea	Mean (m)	STE (m)	STD (m)	MIN (m)	MAX (m)	# cells	Sum (km³)	STE (km³)	[−]: palaeo-DEM above present (on average, in the zone considered) [+]: palaeo-DEM below present (on average, in the zone considered)
Full study area: modern DEM versus palaeo-DEM cross-comparison													
Inactive zone	3545	79.0%	503	14%	0.02	0.09					0.02	0.05	
Lower Valley South ('Cologne')	897	20.0%	180	20%	−0.10 (−0.66)	0.05	1.67	−18.9	36.0	358,501	−0.09	0.04	[−]: net removal/deepening: building activity; aggregate mining
Lower Valley North ('West-Ruhr')	1394	31.1%	198	14%	0.04	0.13	2.57	−31.4	73.6	556,313	0.06	−0.06	[+]: net accumulation/raising: building activity; coal mining dumps
Upper Delta plain ('floodplain rim')	958	21.4%	78	8%	0.05	0.03	0.59	−14.3	28.2	372,920	0.04	0.03	[+]: net accumulation/raising: 9th–19th cy floods and dike breaches; building activity
Upper Delta plain centre ('Betuwe')	296	6.6%	47	16%	0.23	0.05	0.90	−4.1	27.3	112,648	0.07	0.01	[+]: net accumulation/raising: 9th–19th cy floods and dike breaches; building activity
Active zone	942	21.0%	204	22%	0.32	0.42					0.07	0.13	
Lower Valley South ('Cologne')	140	3.1%	24	17%	−0.82 (−0.60)	0.42	4.45	−13.7	33.8	56,188	−0.12	0.06	[−]: net removal/deepening: river bed erosion; river management
Lower Valley North ('West-Ruhr')	172	3.8%	43	25%	0.86	0.43	3.96	−12.5	39.2	68,917	0.15	0.08	[+]: net accumulation/raising: sedimentation; harbour works Ruhrort/Duisburg
Upper Delta ('apex and IJssel')	399	8.9%	61	15%	−0.03	0.42	0.93	−11.2	31.5	149,107	−0.01	0.17	[−]: net removal/deepening: 9th–15th cy incision after avulsion
Upper Delta ('embanked floodplain')	230	5.1%	77	33%	1.23	0.43	2.96	−7.0	19.6	76,604	0.28	0.10	[+]: net accumulation/raising: sedimentation; anthropogenic raised grounds
Full study area	4486	100%			0.09	0.19					0.09	0.13	
Non-stripped area (coal-mining subs.)[a]	3779	84.2%			(−0.25) 0	0.07	1.56	−31.4	31.5	1,480,264	0	0	combination of "West-Ruhr' subsidence and active zone interpolation net −0.25 m
Stripped and void-filled (linear features)	310	6.9%			(0.31) 0.56	0.24	2.36	−28.9	18.7	124,106	0.17	0.07	[+]: net accumulation/raising: raised roads and dikes ≫ entrenched roads
Stripped and void-filled (pos. relief areas)	223	5.0%			(1.7) 2.0	0.58	4.30	−14.3	73.6	85,484	0.45	0.13	[+]: net accumulation/raising: urban and industrial terrains near the river; dump sites
Stripped and void-filled (neg. relief areas)	174	3.9%			(−2.7) −2.5	0.58	3.55	−18.0	12.8	61,344	−0.43	0.10	[−]: net removal/deepening: harbours; aggregate mining near and away from the river
Stripped and void-filled (all features)	707	15.8%			0.27	0.46	3.27	−29	74	270,934	0.19	0.10	[+]: net accumulation/raising
Lower Valley North: cross-comparison H&Z 2014 and coal-mining subsidence correction													
Raw elevation difference 1892–2010 (obtained from Harnischmacher and Zepp, 2014 dataset, overlaps 39% of Lower Valley North)													
Inactive + active zone	611	13.6%			−1.49	0.21							
Inactive zone (overlap area)	516	11.5%			−1.35	0.17	3.92	−27.0	74.4	206,506	−0.69	0.09	[−]: net removal/deepening
Active zone (overlap area)	94	2.1%			−2.28	0.39	3.81	−12.1	38.5	37,674	−0.21	0.04	[−]: net removal/deepening
Coal mining-attributed subsidence component (elevation change in non-stripped subarea, representative for entire H&Z 2014 overlap area)													
Inactive zone (overlap area)	518	11.5%			−1.83	0.11	2.42	−27.0	0.0	207,159	−0.95	0.06	[−]: accommodation space created since 1892
Active zone (overlap area)	94	2.1%			−2.86	0.31	2.97	−12.1	0.0	37,695	−0.27	0.03	[−]: accommodation space created since 1892
Residual elevation change in H&Z 2014 overlap area (raw minus coal mining-attributed component)[a]													
Inactive + active zone	611	13.6%			0.50	0.25							
Inactive zone (overlap area)	517	11.5%			0.49	0.20	*calculated, not queried*				0.25	0.11	[+]: dominantly positive-relief anthropogenic landforms since 1892
Active zone (overlap area)	94	2.1%			0.58	0.50	*calculated, not queried*				0.05	0.05	[+]: dominantly positive-relief anthropogenic landforms since 1892
Remaining part of Lower Valley North (outside H&Z 2014 overlap area, 61% of Lower Valley North)[a]													
Inactive + active zone	955	21.3%			−0.10	0.25							
Inactive zone (nonoverlap area)	877	19.5%			−0.22	0.22	*calculated, not queried*				−0.19	0.19	[−]: net removal/deepening
Active zone (nonoverlap area)	78	1.7%			1.20	0.66	*calculated, not queried*				0.09	0.05	[+]: net accumulation/raising

[a] Mean elevation and volumetric change estimates are negated for coal mining-attributed subsidence affecting modern elevations in the Lower Valley North. Where applicable, raw elevation difference values are given in brackets. Note that elevation and volumetric change estimates still include substantial negative relief of surficial aggregate mining and positive relief of mining waste dumps.

IJssel' subareas are labelled as 'hybrid' methods in our tabulated results in the next section and are reported separately from the ordinary inactive zone (floodplain rim) and active zone (embanked floodplain) in the upper delta (Fig. 8; Table 3).

To generate aggregated results relatively fast computationally, and to remove small artefacts caused by vector-grid conversions in clipping procedures, active-inactive zone boundary digitizing accuracy, and resulting interpolation artefacts, we resampled the final palaeo-DEM to a resolution of 50 × 50 m. We deployed Zonal Statistics and Zonal Histogram operations to summarize the elevation differences between the palaeo-DEM and present-day DEM, broken down to (i) Lower Valley South, Lower Valley North, and Upper Delta (Fig. 8), (ii) inactive zone and active zone (as introduced above), (iii) non-stripped and stripped areas (linear anthropogenic features, negative anthropogenic relief areas, positive anthropogenic relief areas), and (iv) including separate treatment of the elevation change caused by underground mining-induced land subsidence (from Lidar DEM to Input DEM, Fig. 4) and elevation change caused by superficial anthropogenic relief modifying activities (from Input DEM to final DEM, Fig. 4).

Where we report mean values, we also provide an associated standard error (STE, Table 3). We calculated this as a sum of error contributions. The first component is based on the standard deviation (STD) reported in the cell statistics of the DEM-of-difference and calculated as $STD * (N_{cells} - 1)^{-0.5}$, where N_{cells} is the number of cells that contributed to the difference (e.g., all void-filled cells, all subsidence-corrected cells). The second component is the uncertainty of the LiDAR surface, which was set to 0.05 at 5 × 5 resolution, multiplied by $(M - 1)^{-0.5}$ where we resampled to 10 × 10 and 50 × 50 m, with M representing the number of 5 × 5 m cells. The third component is the uncertainty associated with interpolations deployed in void-filled areas and the active zone. This was set to 2 m at 5 × 5 m resolution for the cells affected, multiplied by $(M - 1)^{-0.5}$ at resampled resolutions. The summed standard error for each reported mean was calculated per subarea as the combined components' root sum of squares, and as an area-weighted mean when aggregated to a larger area. Besides elevation change, we calculated volumetric change per subarea to allow further intercomparison of zonal DEM-differences, propagating the standard errors (Table 3).

To serve a palaeohydrological-oriented evaluation of the palaeo-DEM product, we quantified and visualised connected floodplain areas in both the present LiDAR DEM and the palaeo-DEM. We detrended the DEMs with the same second-order polynomial trend surface and sliced the resulting rasters at vertical intervals of 0.5 m. For each interval, we identified all cells of the DEM below the slice and subsequently separated the patch of cells connected to the river. We reused the trend surface created earlier in the workflow to identify and separate positive and negative antropogenic relief. Because this trend surface was fitted on the extended floodplain, excluding insular remnants of Middle Pleistocene elevated terrain and linear elements of anthropogenic origin (Section 4.3), it doubled as a first-order approximation of a flooding water surface during the passage of a high discharge event.

5. Results

In this section, we first report the amount of anthropogenic modifications removed from the LiDAR data to arrive at the palaeo-DEM (Section 5.1). We then proceed to analyse differences between the past and present geomorphology, regarding fluvial dynamics (Section 5.2), and floodplain connectivity in a simple palaeohydrological analysis (Section 5.3).

5.1. Elevation change and volume of anthropogenic elements

Fig. 8 and Table 3 show a tri-partitioned study area that is further subdivided based on treatment in the palaeo-DEM construction workflow. The inactive zone covers 79% of the study area (3545 km^2) and the active zone 21% (942 km^2). In total, 707 km^2 (15.8% of surface area; Table 3) was removed by LiDAR DEM stripping and replaced with interpolated elevations, i.e., the first half of the workflow (Fig. 4). Of this area, 310 km^2 was removed as anthropogenic linear voids (roads, railroads, dikes), 223 km^2 as negative relief non-linear voids (digging, extracting) and 174 km^2 as positive relief non-linear voids (raising, building, dumping). These steps corrected topography throughout the study area with modest differences between southern and northern subzones, but more in the areas close to the river (Table 3: 14% of the inactive zone, 22% of the active zone), and also more in densely populated areas (Fig. 8: shades of grey). This is mainly because these areas host more surface modifications (harbour complexes, aggregate mining) and have denser infrastructure networks, such as in and around the city of Cologne (Fig. 9).

In the inactive zone, the stripping and void filling resulted in a very minor net mean elevation change of 0.02 ± 0.09 m for the full study area (Table 3). This is the result of a cancelling-out effect between the southern and northern parts. The Lower Valley South ('Cologne') shows negative elevation change of −0.10 ± 0.05 m (net removal), whereas the Upper Delta plain in its central parts ('Betuwe') shows a positive elevation change of +0.23 ± 0.05 m (net accumulation), attributable to sedimentation by ninth–nineteenth cy floods and dike breaches besides anthropogenic sediment import (e.g., aggregate mining from the active zone).

The determination of elevation change for the middle part of the study area ('West-Ruhr') is more complex, because of a subsidence component caused by underground mining. Raw quantification suggests a net lowering of −0.66 ± 0.13 m over the full Lower Valley North (1394 km^2). In the 'West-Ruhr' industrial subarea where our study area overlaps the H&Z 2014 dataset (Harnischmacher and Zepp, 2014), the net change totals −1.35 ± 0.17 m (516 km^2). Using that dataset (difference between LiDAR DEM and Input DEM) and our areal subdivisions in 'natural' topography (not stripped) and anthropogenic modified topography (stripped and void-filled), we split an estimate of subsidence (sampled in the non-stripped area and held representative for the neighbouring stripped areas) from the total elevation change. For the H&Z 2014 overlap area, the sampled subsidence-attributed and calculation-derived (residual) elevation change components are reported seperately (Table 3). The subsidence-attributed component is only considered in the H&Z 2014 overlap area (13.6% of full study area; 39% of Lower Valley North; mean value over this area: −2.0 ± 0.14 m). Being able to separate human-induced subsidence from direct human modifications to the terrain ratifies our choice to correct for this subsidence before further reconstruction (Fig. 4). In addition, it illustrates one of the advantages of having clearly defined steps and intermediate output in the workflow. To help cross-comparisons of changes between subareas, the subsidence component is kept out of the further tabulated results for mean elevation and volumetric changes (Table 3). This yields a modest net positive change of 0.04 ± 0.03 m in the inactive zone of the Lower Valley North (+0.49 ± 0.20 m in the subsidence-affected subarea; cancelled out by −0.22 ± 0.22 m in the remainder).

All in all, the inactive zone shows a modest loss of relative elevation since early medieval times in the southern Lower Rhine valley (urbanized terraced valley floor), lots of activity and complications of subsidence but near-zero net change in the middle reaches (urbanized and industrialized valley floor), and a modest gain in the downstream deltaic reaches (flooding-protected urbanized upper delta plain). This result is in line with general expectations when evaluating mean values of anthropogenic change between a palaeo-DEM and a present-day DEM over very large areas of river valley: it complies with the idea that the bulk resources to raise terrains were obtained from within the valley floor. This is best illustrated by the volumetric break-down of elevation change to the zonations of the DEM-stripping steps. Cells representing positive-relief anthropogenic landforms total 0.45 ± 0.13 km^3 above the void-filled palaeo-DEM surfaces, and linear features

(raised roads, dikes) add another 0.17 ± 0.07 km^3 (Table 3). The counter-balance volume extracted from negative landforms totals 0.43 ± 0.10 km^3, which we consider a minimum value because many sand pits are deeper in reality than in the Input DEM. Calculating volumes of anthropogenic elements was possible because we stripped these elements prior to our reconstruction of the active zone.

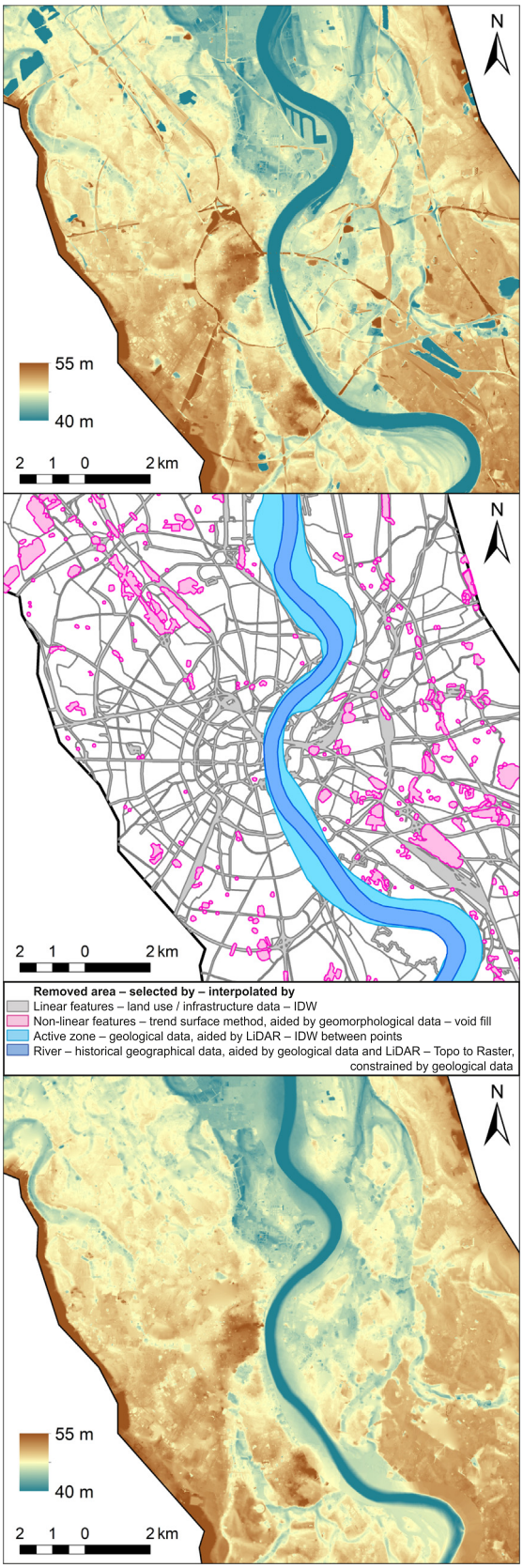

Fig. 9. Detail of study area around Cologne with LiDAR DEM (top), altered surface areas separated by method (middle), and palaeo-DEM (bottom).

5.2. Active zone and river position

The active zone covers ~20% of the study area (Fig. 8). The width of the active zone is approximately 1 km in the southern part of the Lower Rhine valley and increases to 2 to 3 km in the northern part. The active zone splits in the delta, where the three parts of the active zone each measure 1 to 2 km in width. The study area itself is also less wide along the terraced upstream reach of the Lower Rhine than it is in the delta apex region. In most of the study area, about 15% of the width has been reworked by fluvial activity since 800 CE.

The reconstructed river position (Section 4.4) provides an overview of Lower Rhine meander dynamics in North Rhine-Westphalia and the Netherlands (Fig. 10). As already known from geological mapping at a longer Holocene time scale (Klostermann, 1992; Erkens et al., 2011), lateral meander migration was restricted in the southern part of the study area, but considerably increased downstream. This explains the downstream increase in river position changes and the widening of the active zone (Fig. 10). Especially in the Dutch-German border region, the Rhine and its branches were dynamically meandering, with bends migrating downstream and repeatedly cutting themselves off (Hoppe, 1970; Kleinhans et al., 2011; Verhagen et al., 2017; Overmars, 2020). Hence, the active zone is fairly wide in this area.

Beyond the apex region, i.e., downstream of Nijmegen and Arnhem, the active zone is essentially equal to the embanked floodplain areas between the rivers and the dikes. Here, the active zone width narrows and straightens compared to upstream in the delta apex (Fig. 8). In part this

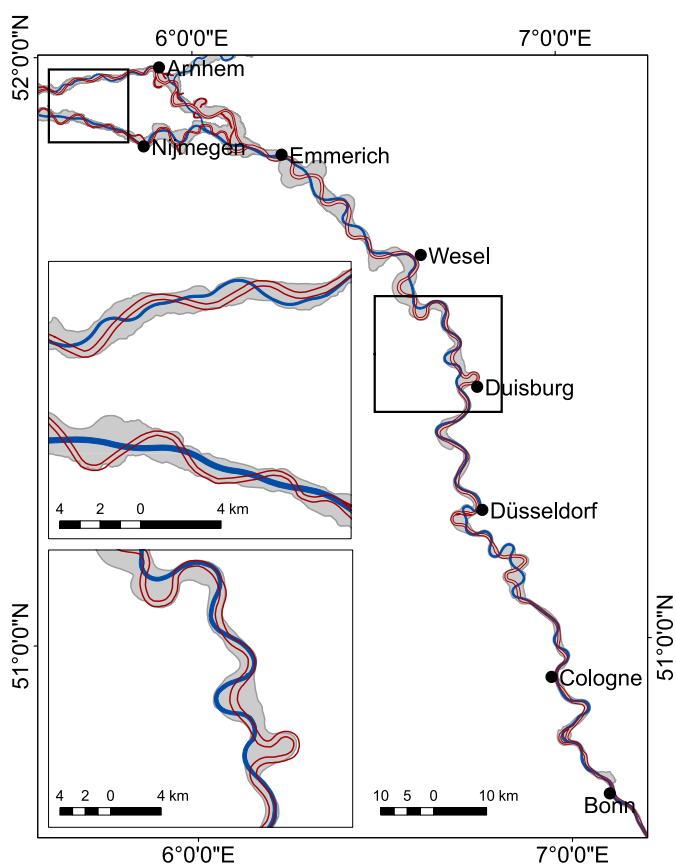

Fig. 10. Reconstructed channel positions for the target age (red, hollow) and present river channels (blue, solid), within the palaeo-DEM's active zone (grey). Insets show the active zone and river positions in more detail for a middle and a downstream portion of the study area.

is because of deltaic substrate characteristics and the discharge division over multiple branches (Berendsen and Stouthamer, 2001; Stouthamer et al., 2011), but more importantly because of river embankment, which confined meander activity. Embankment started centuries earlier in the downstream parts of the study area (eleventh–twelfth cy; e.g., Heunks and Van Hemmen, 2016) than in the apex region (thirteenth–fourteenth cy; sources above). The positions of later historic to modern dikes (eighteenth–nineteenth cy) and hence the widths of the delta's embanked floodplains were determined not so much by medieval embankment quality but by changes in discharge partitioning over the branches (Kleinhans et al., 2011; Verhagen et al., 2017).

Quantification of net elevation change in the active zone bears greater uncertainties than in the inactive zone, and the interpretation is more complex because aspects of channel migration and anthropogenic activities interplayed. Averaged over the full study area, the palaeo-DEM implies a modest positive elevation change $+0.32 \pm 0.42$ m (Table 3), but this value shows large differences when broken down for upper, middle and lower reaches. In the Lower Valley South ('Cologne'), the active zone lost floodplain and bed elevation (-0.82 ± 0.42 m), matching insights regarding channel bed incision in this reach (Erkens et al., 2011; Frings et al., 2019). Contrarily, the active zone in the Lower Valley North shows a net raising of the surface ($+0.86 \pm 0.43$ m). For some parts, this can be attributabed to fluvial deposition in the proximal floodplain, but for the greater part it should be regarded as an outcome of human action (Duisburg-Ruhrort main inland harbour complex; e.g., Krause, 2003). The embanked floodplains in the Upper Delta show a net gain in surface elevation of 1.23 ± 0.42 m. This large change is attributable to floodplain sedimentation in between the dikes, which even necessitated further raising of these dikes (e.g., Hudson et al., 2008). The implied surface elevation change in the IJssel branch subzone is modestly negative and should be seen as the effect of comparing a situation without an incised river channel to one with a mature channel.

5.3. Floodplain connectivity

In the present situation, many low-lying areas are separated from the proximal floodplain of the Rhine and from each other by dikes and other types of artificial features. These features form topographic barriers by crossing flat terrain and low corridors such as residual channels in Late Pleistocene terraces (Fig. 9A). This is not the case in the palaeo-DEM, where the removal of anthropogenic structures implies that floodplain connectivity was much higher (Fig. 9C). Indeed, the surface area that is connected at varied inundation levels greatly differs between the present and past situations (Fig. 11). This illustrates a difference in potential inundation extents between early medieval and recent times.

The differences in river-connected floodplain are most developed in the middle range of the inundation levels. When the detrended DEMs are sliced at −4 m, only the river channels themselves and isolated basins are at the inundated level, and the surface area connected to the river is similar in the present and past situations (Fig. 11A). At higher inundation levels, increasingly larger parts of the floodplain are connected to the river in the palaeo-DEM compared to the present situation. Note that the total area below the detrended surface is roughly similar in both DEMs (Fig. 11B), but the large difference is in the size of the area connected to the river (dark blue patch in Fig. 11B; $0.67 * 10^3$ versus $2.11 * 10^3$ km^2).

Especially in the northern half of the study area with extensive dike networks, inundated floodplain areas were much larger in 800 CE than at present. In the early historic natural situation, a larger proportion of surface area was flooded regularly in this downstream area than along the upstream terraced reaches. This confirms geological, archaeological and historical information on past flood extents, and our incorporation of these materials in the study (Table 1). These spatial differences have important implications for e.g., the mapping and intercomparison of human settlement and overbank sedimentation patterns within the larger study area.

Simple trend surface-slicing (i.e., the results in Fig. 11) in its approach to assess inundation and connectedness does not take into account many important hydraulic control factors, such as surface roughness and flow patterns, and strongly depends on the applied trend surface and its resolution. Analysis of inundation and connectedness can be refined by applying 2D palaeoflood hydraulic models (e.g., Hesselink et al., 2003; Alkema and Middelkoop, 2005). These require as main input an accurate reconstruction of floodplain topography, such as we present here. Our exploratory analysis demonstrates the importance of incorporating palaeotopography in hydraulic modelling studies aimed at quantifying past flooding patterns, flood water levels and discharge magnitudes. The reconstruction of paleo-DEMs is not just useful as terrain input for paleohydrological simulatios. The trend-sliced surfaces can also provide a floodplain landscape zonation template, which is useful when a vegetation reconstruction is needed (e.

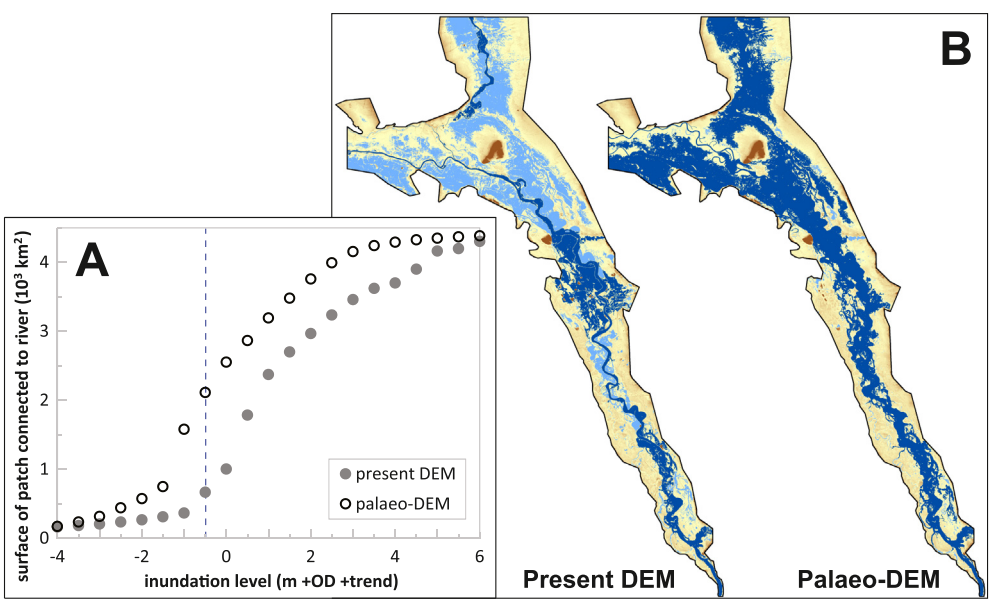

Fig. 11. A) Surface area of the detrended floodplain connected to the river at varied inundation stages. B) Detrended present and past floodplain at an inundation level of −0.5 m (near-maximum difference in connectivity). Blue patches are below this level, with dark blue indicating the surface area connected to the river.

g., Brouwer Burg, 2013), for instance to provide palaeoflood model scenarios with spatially-distributed hydraulic roughness values.

6. Discussion

6.1. Information intake in palaeo-DEM construction methods

In this section, we first evaluate the relative importance of the different steps in our workflow. This serves to evaluate the top-down approach taken up in this research to produce palaeo-DEMs for large riverine study areas for historic and prehistoric periods, for mapping and modelling applications in fluvial geomorphology and palaeohydrology. The information intake comprised datasets with direct dating information (Section 4.2), but also a considerable number of present-day datasets in which age information was at best implicit. We then focus on how these were combined, and how it works out methodologically if one wants to repeat such work for different river valleys or adapt it for considerably younger or older target periods.

Section 5.1 and Table 3 present summarized metrics on the accumulated elevation differences between the palaeo-DEM and the Input LiDAR DEM, amongst others broken down between the inactive and active zones. In the inactive zone, the palaeo-DEM results only from DEM-stripping methods, i.e., the upper half of the workflow (Fig. 4). This part of the workflow is a fully top-down approach, also called retrogressive (Werbrouck et al., 2011) and deductive (Schmidt et al., 2018). These stripping steps utilise present-day mapping of anthropogenic features (Section 4.3). The preceding subregional mining-subsidence correction utilises existing data on present vs. late-nineteenth cy elevation differences (Section 4.1). Importantly, both the stripping and warping steps do not depend on specification of an exact target age for the palaeo-DEM. As such, the palaeo-DEM result for the inactive zone does not have an explicit date stamp associated to it. Rather, it represents a landscape before major anthropogenic impacts on the topography. For the early historic (circa 800 CE) target period in our study area, such an approach is defendable and appears sufficient to reconstruct the palaeotopography in the inactive zone. This is not the case for considerably older and considerably younger target ages (see Section 6.4).

Querying current land-use data on anthropogenic features is the preferred method for DEM stripping, because it can be automated after determining buffer widths manually. For a large study area, however, choice and availability of land-use datasets are limited by their uniformity, completeness, and precision. The geometry of the features in the datasets has to be precise to remove only the undesired parts from the LiDAR product, and at least as accurate as the cell size of the DEM that is stripped (5×5 m in our case). In our case, we largely overcame initial problems with dataset inaccuracy by resampling the end result to cell sizes an order of magnitude coarser. Another limitation is that typical land-use datasets are not primarily classified by morphology and therefore often do not provide accurate boundaries of anthropogenic terrain elements. We found that in our study area this is not a major problem for linear features. In particular, the infrastructure vector lines from OpenStreetMap, almost perfectly follow the middles of entrenched and raised segments (Fig. 5A). Based on this experience, we regard the infrastructure data well-suited for use in automated DEM-stripping, probably also in other geomorphological environments. Other, mostly non-linear elements are of many different types and seldom consistently classified in existing maps and datasets. Despite the considerable number of land-use datasets available for the Netherlands and Germany, we did not make direct automated use of these. Due to the lack of explicit morphological attributes in common land-use datasets, besides local geometric difficulties in homogenizing partial datasets by different original makers, our workflow uses a trend surface-aided manual identification for further DEM stripping.

The trend surface-based method relies on the detection of anthropogenic elements based on their deviating elevation, and can be used to remove all remaining anthropogenic elements from the topography. Critically, the workflow begins this step after removing linear features by land-use datasets and any corrections for mining subsidence. This is convenient for three reasons. First, the trend surface improves when some anthropogenic elements are already removed. Second, this workflow order saves time as the trend method relies upon manual selections to remove features. Third, it restricts the more subjective manual identification steps to a smaller number of features. Although it is generally straightforward for a geomorphologically-trained eye to determine whether an element on a DEM is natural or anthropogenic, and this identification process is aided qualitatively by cross-referencing between the detrended LiDAR DEM and satellite imagery the number of elements can be overwhelming and mistakes are possible.

The production methods and results for the active zone in our palaeo-DEM are more of a restorative effort than a stripping one. The resultant topography in the active zone derives from the present morphology (Fig. 7), but our methods for distinguishing the active zone as well as our methods for reconstructing the past river geometry incorporate various types of additional data (Fig. 3; Table 1) and reasoning. The results for the active zone are more uncertain than those for the inactive zone. This outcome was clear from the start of the research. The need to demarcate the active zone from the inactive zone is evident in the proportionally larger volumetric differences between the present and the palaeo-DEM (Section 5.1Table 3). It is also clear from the larger demands on information needed to reconstruct the landscape of the active zone. The additional information intake besides the Input DEM (used to manually sample point elevations to interpolate a floodplain topography) were the geological and archeological mapping studies used to define the active zone edges and palaeochannel positions. In contrast to the methods for the inactive zone, those for the active zone demand an explicit specification of the palaeo-DEM target age. Because of the insertion of the river channels, the demarcation of the boundary with the inactive zone, and the iterative 'sculpting' nature of the active-zone floodplain interpolation, the palaeo-DEM is not the product of a fully top-down approach. Neither, however, is it the result of a fully bottom-up approach. The recent reworking that defines the active zone means that it is a large void area asking for restorative decisions either way. The active zone workflow steps can be framed as a hybrid methodology (just as we framed the workflow for the deltaic parts in the study area; Section 4.5; Fig. 8).

6.2. Accuracy of palaeo-DEM and outlook on validation

Here, we describe the implications of the methodological choices on accuracy of the palaeo-DEM and validation opportunities. We present the final palaeo-DEM and elevation differences relative to the present (Table 3) at a downsampled resolution of 50×50 m. Zooming to 5×5 m production resolution, the palaeo-DEM reveals various minor anthropogenic features (shallow ditches and small roads; Fig. 5C; Fig. 6F) that neither the linear nor the non-linear stripping procedures removed. In theory, one could apply either stripping method at a small spatial scale to eliminate this reason for downsampling. For a small study area (12.5 km^2 in southern Germany), with the isolation of a subtle local topographic saddle as the goal, Schmidt et al. (2018) provided a palaeo-DEM construction example using a stripping and void-filling approach that also removed many minor anthropogenic elements, for example by buffering each field boundary. However, the risk associated with removing many buffered features is that void-interpolation becomes difficult. The larger the proportion of voids, the smoother the interpolated palaeo-DEM becomes, but such a smooth surface does not represent a realistic state of the landscape (Reuter et al., 2007). The reconstructed terrain in our active zone is relatively smooth for a similar reason. This is hard to avoid for areas where palaeotopography is missing due to erosion (Schneider et al., 2017).

For applications where field-scale feature isolation is not the goal, downsampling a stripped DEM is the practical solution, given that the

elevation differences of smaller anthropogenic elements with respect to their surroundings are usually minor (Fig. 5C; Fig. 6F) and the material dug from ditches is often incorporated in the elevation of the surrounding land. When the foreseen application is valley-scale palaeohydrological modelling, a resolution of 50 m is still significantly finer than typical grid sizes of numerical models, which are limited for computational reasons.

The vertical resolution at which the reconstruction is accurate is less straightforward to assess than the horizontal resolution. For the method of DEM stripping by land-use datasets, the vertical accuracy of the intermediate result (DEM I) is as good as that of the LiDAR DEM, which is in the order of 0.05 m. Section 4.5 and Table 3 report how this uncertainty propagates into zonal elevation-difference averages and volumetric totals. This section discusses vertical accuracy of the palaeo-DEM at the individual cell scale. This varies across the study area because (i) different stripping and void-interpolaton methods were applied and (ii) subareas differ in history and degree of anthropogenic modifications.

In parts of the study area, the palaeo-DEM infers surfaces for the target age currently buried below younger relief. In these places, at least in theory, one could locally validate the reconstruction in an excavation or borehole, or against existing detailed cross-sections encountered occasionally in literature (e.g., Krause, 2003). However, for the majority of stripped and interpolated cells (e.g., the active zone and the areas of negative relief in the inactive zone: some 25% of the full study area), the palaeo-DEM is restorative and cell-based verification cannot be performed. Quantitative trust in the quality of the palaeo-DEM for this area thus needs to derive from zonal averaged and intercompared elevation differences as presented in Table 3 and Section 5.1.

For cells affected by the trend surface-based method deployed to identify positive and negative relief elements (Section 4.3), the vertical accuracy depends on the size of the interpolated voids and on the choices made in the reclassification step. We reclassified the detrended DEM at 0.5 m height intervals; therefore, anthropogenic elements with an elevation deviating less than 0.5 m were not identified nor removed in this step. The largest areas of (potential) anthropogenic positive elevation that remain in the palaeo-DEM are those underneath the centres of towns and cities. Many of these were founded in late medieval times (i.e., after our target age), although Cologne is a marked exception of Roman age. The inner parts of large old cities are likely the locations where the vertical accuracy is lowest. Here, upgrading the cell-by-cell accuracy of the palaeo-DEM is possible, but requires a bottom-up approach utilising detailed archaeological stratigraphy with dating control throughout the city centres. Given the large size of our study area, this is not feasible. Improving the accuracy at this resolution is necessary for small-scale applications, such as mapping past urban topography (Gerlach, 2003; Krause, 2003; Baubiniene et al., 2015; Mozzi et al., 2018), but for typical regional-scale applications (e.g., Section 5.3) reconstruction at such detail is not required.

Within the inactive zone, the restorative terrain interpolations produce smoothed floodplain landscapes (Fig. 7D), which include terrace scarps but do not further account for variations in topography caused by natural processes. Activity of smaller streams and mass movements at terrace edges, for example, are not regarded and neither is point-bar ridge-and-swale topography. The relatively smooth active zone palaeo-DEM could be used as starting point to simulate such micro-relief when an application demands it.

In the most downstream parts of the study area, hybrid methods of palaeo-DEM construction were deployed (Section 4.5). These included assumptions on gradual aggradation of the floodplain in areas outside the active zone (complying with Pierik et al., 2017), a process that largely ceased after embankment. Because our target age is close to the moment of embankment in the delta, the resulting corrections and their vertical inaccuracy are small: generally centimetres, but closer to the river locally up to decimetres. Especially in these areas, the palaeo-DEM can be verified and improved by integrating newly-processed subsurface data to determine the thicknesses of historic sediment packages at many locations (e.g., Vermeer et al., 2014; Pierik et al., 2018). Doing so would change the hybrid workflow from a dominantly top-down approach to a dominantly bottom-up approach, significantly increasing data requirements (Section 1). Furthermore, the top-down approach performs well in a rather uniform way for both the deltaic and the valley parts of the study area, while bottom-up approaches are expected to differ strongly between these settings.

6.3. Applicability to other study areas

The top-down palaeo-DEM construction workflow is generic in set-up and therefore transferable to other lowland areas and other target ages. The relative importance of the different workflow steps and required input data, however, may shift when the workflow is applied to cases and periods older or younger than the Rhine in early historic times (Fig. 12).

The workflow can be applied to construct large-scale palaeo-DEMs for other lowland areas if a high-resolution LiDAR DEM is available. In addition to being the starting point for stripping the present topography, the LiDAR DEM helps to define the active zone in combination with geological data, and to reconstruct the river position in combination with historical information. Removal of anthropogenic elements (DEM stripping) was the most important step in our reconstruction of the Lower Rhine valley and we expect this to be similar in other cases, because lowland areas are generally densely populated with long settlement histories, resulting in abundant anthropogenic modifications to the terrain. DEMs removed from such features can provide valuable starting points for archaeological prediction maps (Cohen et al., 2017) and modelling studies that focus on human-landscape interactions in deltas (Groenhuijzen and Verhagen, 2017; van Lanen et al., 2018). In sizeable study areas centred around meandering rivers, it is important to also consider the extent of the active zone. As this zone requires restorative steps, geological data to mark the edges of the zones and geomorphological insights to decide on the filling are indispensable tools for reconstruction. Still, for the active zone conducting DEM stripping is advisable before starting other operations because it improves recognisability of natural geomorphological features (Figs. 5 to 9).

6.4. Applicability to other time periods

The workflow adequately removes anthropogenic features and restores a palaeo-DEM representing the time before major anthropogenic modifications to the terrain. The timing of this moment may be significantly different in other study areas as it is related to population density and technological developments. For example, in most of the Americas, significant anthropogenic modifications did not start before 1800 CE, whereas in some parts of Africa, Asia, and Europe, the first large (visible in a 50 × 50 m cell-size DEM) anthropogenic geomorphological elements are considerably older than 800 CE. The absolute age of this moment is important to assess which approach, procedures and data are relevant when constructing the palaeo-DEM (Fig. 12). Decisions on a target age also affect the accuracy at which one can reconstruct the morphology of the active zone, and whether the main resources to do so are historic observational data and maps, or geological and geoarchaeological data. In the case of the Lower Rhine, target ages in Roman to medieval time (with our 800 CE moment a mid-point of that) imply using a combination of both (for reasons listed in Section 3). This is methodologically illustrative in general, but necessitates steps in the workflow (Fig. 4) that are likely not relevant to readers having palaeo-DEMs for either the youngest centuries or for many millennia older in mind (hence, Fig. 12).

Historical data will play an increasingly important role when elements of the workflow are applied to periods younger than the first anthropogenic modifications. For recent periods (circa 1850 and later), a palaeo-DEM may be constructed based solely on historical elevation and bathymetry data. This may be especially useful for the more difficult

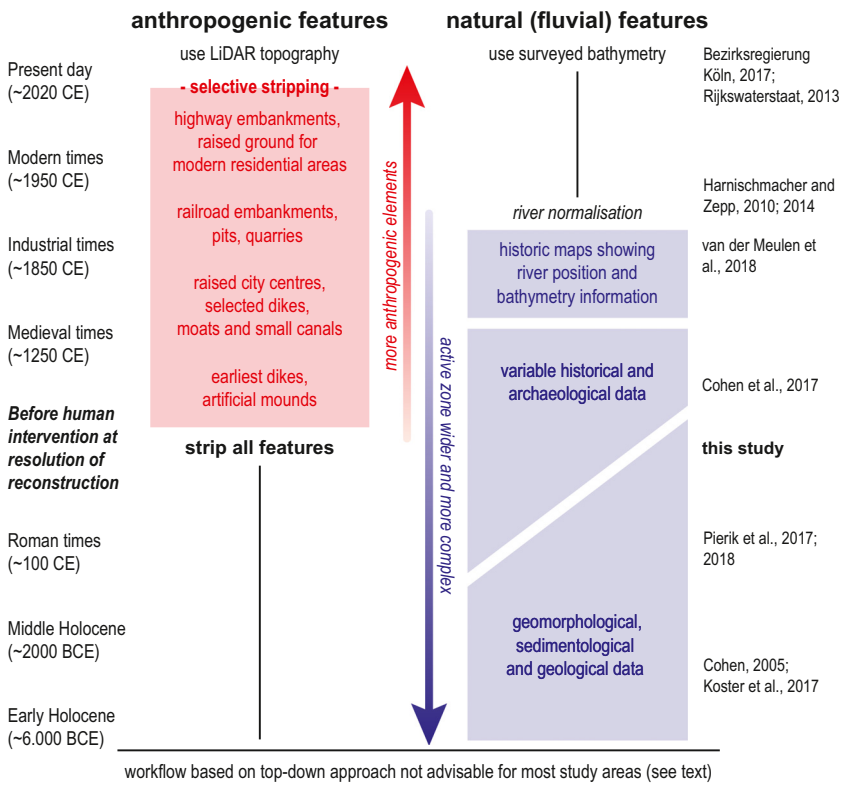

Fig. 12. Overview of changes to the workflow and data intake when it is applied to older or younger time periods. The periodization varies per study area, therefore the left column gives this in broad terms, with ages in brackets indicating the particular timing in the Lower Rhine valley. References in the right column are palaeo-DEM construction studies relevant to the study area.

reconstruction of geomorphologically active zones (van der Meulen et al., 2018; Overmars, 2020) and urban environments (Krause, 2003; Wronna et al., 2017). The accuracy and effective resolution of the resulting DEM will reflect those of the historical data. This possibility depends on the availability of such data (only specific study areas) and cannot be used to correct for elements older than the data itself; for example, the river dikes in our study area predate any quantitative measurement data by many centuries. For palaeo-DEMs of late medieval or early modern times, a combination with the workflow presented here is possible.

When stripping methods are deployed to younger periods of human history, the filtering of anthropogenic modifications has to be conducted selectively (Fig. 12). Although most anthropogenic changes to the terrain occurred during the nineteenth and twentieth centuries, there are major exceptions such as dikes, raised settlements, and canals (e.g., Schmidt et al., 2018). Determining which features were present, and reconstructing their correct dimensions, requires integration with historical data. These data need to inform on ages of elements as well as their geometrical evolution over time. A higher temporal resolution is required for more recent historical periods, when rates of anthropogenic alterations increased. In short, our top-down workflow concepts are well applicable to palaeo-DEM construction for younger time periods, but in practice using them will be harder because the stripping steps have to be selective. The active zone, on the other hand, is smaller and easier to reconstruct, because the effects of geomorphological processes such as erosion are smaller over shorter time scales (and one may even have direct historical observational data available on lost features; e.g., Overmars, 2020).

Farther back in time, a greater area has been reworked and hence the area to be considered the active zone is enlarged. As a result, restoration of the active zone will require more assumptions. Therefore, geological and geomorphological information play an increasingly important role for earlier palaeo-DEM target periods (Fig. 12). The workflow for the inactive zone does not require any new input when targeting earlier periods; it only becomes smaller at the expense of the active zone.

For palaeo-DEMs with target ages predating the Holocene, we regard that the top-down approach loses its benefits compared to bottom-up approaches. In our study area, this is because the active zone then becomes so wide that it covers a major part of the valley floor, and only few preserved remnants can be considered indicative of the palaeotopography, especially in the centre of the valley (e.g., Erkens, 2009). Furthermore, in the remainder of the study area one should account for geomorphological processes of a different nature than fluvial reworking, such as periglacial colluvial and aeolian activity. For study areas in different parts of the world, geomorphological responses to external changes in climate and base level determine the adequate lower time limit of the top-down approach. In most lower river reaches this is a moment between the Last Glacial Maximum (circa 21 ka) and the Mid-Holocene optimum (circa 7 ka), because for palaeo-DEM target periods prior to that time most of the region has to be considered as active zone (e.g., Briant et al., 2018).

7. Conclusion

Present-day DEMs alone are not suitable to study past riverine geomorphological processes and events such as historic floods, because parts of the terrain are altered by anthropogenic modifications and natural processes. These parts should be reconstructed in a palaeo-DEM prior to quantitative analysis of past situations. We present a workflow for LiDAR-derived high-resolution palaeo-DEM construction, developed for the case of the Lower Rhine valley and upper delta. Our workflow is suitable to reconstruct the topography of large valley-floor areas (>1000 km^2) at fairly high resolution (5 × 5 m processing resolution; 50 × 50 m output resolution), because it relies upon LiDAR DEM adaption ('top-down' approach). The final palaeo-DEM is regarded to be accurate at a horizontal resolution of 50 m and at a vertical accuracy of ±

0.5 m (considerably better in non-stripped areas, and potentially less accurate locally in the morphologically active zone).

Stripping anthropogenic elements separately from reconstruction in the active zone allowed us to quantify direct human influence in the landscape. The total volume of anthropogenic modification in the Lower Rhine floodplain area is in the order of 10^9 m^3. Positive and negative topographic changes nearly cancel each other out over the 4500 km^2 of valley surface considered (net volumetric change 0.09 ± 0.13 km^3, excluding mining-subsidence related accommodation space). We demonstrate large differences in floodplain connectivity between the past natural situation and the present situation characterized by anthropogenic relief elements, highlighting the importance of incorporating the past topography in palaeoflood research. The palaeo-DEM product and our assessment of its accuracy can potentially be verified locally. However, over some 20% of the study area, it is an informed restorative product that cannot be verified by observational data, but might be validated through its use in modelling work.

The critical first steps of the workflow consist of removing anthropogenic relief elements and filling the resulting voids. These DEM-stripping steps are sufficient to reconstruct the topography of the distal floodplain defined by inherited relief with many anthropogenic modifications, with little explicit demand for hard-to-obtain detailed age information on the anthropogenic features to be removed. The reworked proximal floodplain requires additional steps for which we involved existing historical and geological information, with greater demands on compiled age information (obtained from geological, archaeological and historical sources). Distinguishing these geomorphologically distinct 'inactive' versus 'active' zones is important for reliable palaeo-DEM construction.

Most terrain features that are present on the LiDAR DEM but not on the palaeo-DEM are either highly linear, such as embankments, or highly non-linear (circular or square-shaped), and have relatively sharp and abrupt (steep) edges. This allowed us to identify and remove them in the stripping process, and explains the large difference in approximated floodplain connectivity and potential inundation between the present and the palaeo-DEM.

The workflow developed in this study is widely applicable to other lowland areas at different spatial scales and resolutions, and the workflow can be adjusted for the palaeo-DEM to represent other time periods. Reconstructions for later periods require selective stripping of the DEM, which demands historical or archaeological data to determine the ages and past dimensions of anthropogenic elements. In contrast, reconstructions for earlier periods require no additional DEM stripping. Compared to the palaeo-DEM for our target age, palaeo-DEMs for considerably older periods in the Holocene (e.g., Bronze Age, Neolithic or Mesolithic situations) increasingly rely on restorative approaches taking in geological and geomorphological data. Overall, the top-down approach is limited to target ages in geologically recent time periods (end of Pleistocene and younger).

Declaration of competing interest

The authors declare that they have no known competing financial interests or personal relationships that could have appeared to influence the work reported in this paper.

Acknowledgements

This study was funded by STW (now NWO-TTW), project 14506. We thank Hessel Woolderink and Maarten Zeylmans for help with processing raw LiDAR data. Stefan Harnischmacher kindly provided digital data for the Ruhr area. We thank the organising committees of the FLAG 2018 and INQUA 2019 meetings, where we presented and discussed our methods and preliminary results. Two anonymous reviewers and the SI editor Cordier are thanked for their constructive criticism and advice on an earlier draft of this manuscript. Journal editor Lecce is thanked for editorial corrections. The palaeo-DEM output, intermediate step products, and all automatic and manually created feature-selection data files used in the production process (lines, polygons, points) are archived and will be made available as open data.

References

AHN2-RWS, 2013. Algemeen Hoogtebestand Nederland (AHN2). Rijkswaterstaat. www.ahn.nl/common-nlm/open-data.html.

Alkema, D., Middelkoop, H., 2005. The influence of floodplain compartmentalization on flood risk within the Rhine–Meuse Delta. Nat. Hazards 36, 125–145.

Baubiniene, A., Morkunaite, R., Bauza, D., Vaitkevicius, G., Petrosius, R., 2015. Aspects and methods in reconstructing the medieval terrain and deposits in Vilnius. Quat. Int. 386, 83–88. https://doi.org/10.1016/j.quaint.2014.09.068.

Bechert, T., 2007. Germania Inferior. Eine Provinz an der Nordgrenze des Römischen Reiches. Verlag Philipp von Zabern, Mainz am Rhein, p. 167.

Begbie, D., Roberts, G., 2014. Bridging in the Second World War: an imperative to victory. Proceedings of the Institution of Civil Engineers-Engineering History and Heritage 167, 111–121.

Benito, G., Díez-Herrero, A., 2015. Palaeoflood hydrology: reconstructing rare events and extreme flood discharges. In: Paron, P., Di Baldassarre, G., Schroder, J. (Eds.), Hydro-Meteorological Hazards, Risks and Disasters, pp. 65–104 https://doi.org/10.1016/B978-0-12-394846-5.00003-5.

Berendsen, H.J.A., Stouthamer, E., 2001. Palaeogeographic Development of the Rhine-Meuse Delta, the Netherlands. Koninklijke Van Gorcum, Assen, p. 268.

Breeze, D.J., Jilek, S., Graafstal, E.P., Willems, W.J.H., Bödecker, S., 2018. Frontiers of the Roman Empire; the Lower German Limes. Sidestone Press, Leiden, p. 143.

Briant, R.M., Cohen, K.M., Cordier, S., Demoulin, A.J.A.G., Macklin, M.G., Mather, A.E., Rixhon, G., Veldkamp, T., Wainwright, J., Whittaker, A., Wittmann, H., 2018. Applying Pattern Oriented Sampling in current fieldwork practice to enable more effective model evaluation in fluvial landscape evolution research. Earth Surf. Process. Landf. 43, 2964–2980. https://doi.org/10.1002/esp.4458.

Brouwer Burg, M., 2013. Reconstructing "total" paleo-landscapes for archaeological investigation: an example from the central Netherlands. J. Archaeol. Sci. 40, 2308–2320. https://doi.org/10.1016/j.jas.2013.01.008.

Brown, A.G., Tooth, S., Bullard, J.E., Thomas, D.S.G., Chiverrell, R.C., Plater, A.J., Murton, J., Thorndycraft, V.R., Tarolli, P., Rose, J., Wainwright, J., Downs, P., Aalto, R., 2017. The geomorphology of the Anthropocene: emergence, status and implications. Earth Surf. Process. Landf. 42, 71–90. https://doi.org/10.1002/esp.3943.

Cohen, K.M., 2005. 3D geostatistical interpolation and geological interpretation of palaeo-groundwater rise in the coastal prism in the Netherlands. In: Giosan, L., Bhattacharaya, J.P. (Eds.), River Deltas: Concepts, Models, and Examples. SEPM Special Publication 83, pp. 341–364. https://doi.org/10.2110/pec.05.83.0341.

Cohen, K.M., Stouthamer, E., Pierik, H.J., Geurts, A.H., 2012. Rhine-Meuse Delta Studies' Digital Basemap for Delta Evolution and Palaeogeography. https://doi.org/10.17026/dans-x7g-sjtw.

Cohen, K.M., Arnoldussen, S., Erkens, G., van Popta, Y.T., Taal, L.J., 2014. Archeologische verwachtingskaart uiterwaarden rivierengebied. Deltares, Utrecht, p. 182 https://doi.org/10.17026/dans-zbt-xcck.

Cohen, K.M., Dambrink, R., De Bruijn, R., Marges, V.C., Erkens, G., Pierik, H.J., Koster, K., Stafleu, J., Schokker, J., Hijma, M.P., 2017. Mapping buried Holocene landscapes: past lowland environments, palaeoDEMs and preservation in GIS. In: Lauwerier, R. C.G.M., Eerden, M.C., Groenewoudt, B.J., Lascaris, M.A., Rensink, E., Smit, B.I., Speleers, B.P., Van Doesburg, J., (Eds.). Knowledge for Informed Choices: Tools for more effective and efficient selection of valuable archaeology in the Netherlands. Netherlands Archeological Reports 55, 73–93.

Denis, S., Gjesfjeld, E., Moreau, L., 2019. Post-Linear Pottery cultural boundary and repopulation of the German Rhineland: revisiting the Western contacts hypothesis. J. Archaeol. Sci. Rep. 23, 946–952.

DGM1-BrK 2017. Digitales Geländemodell (DGM1). Version 2.0. Bezirksregierung Köln. www.opengeodata.nrw.de/produkte/geobasis/dgm/dgm1.

Erkens, G., 2009. Sediment Dynamics in the Rhine Catchment: Quantification of Fluvial Response to Climate Change and Human Impact. Utrecht University.

Erkens, G., Hoffmann, T., Gerlach, R., Klostermann, J., 2011. Complex fluvial response to Lateglacial and Holocene allogenic forcing in the Lower Rhine Valley (Germany). Quat. Sci. Rev. 30, 611–627. https://doi.org/10.1016/j.quascirev.2010.11.019.

FRE-LGL, 2019. Frontiers of the Roman Empire – the Lower Germanic Limes. Nomination File Part I (Leene, T., Bödecker, S., Berger, L., Henrich, P., Polak, M., Eds.). Governments of The Netherlands, North Rhine-Westphalia and Rhineland Palatinate. 255 pp. Last Access: 28-02-2020. www.limeswerelderfgoed.nl/nominatie.

Frings, R.M., Hillebrand, G., Gehres, N., Banhold, K., Schriever, S., Hoffmann, T., 2019. From source to mouth: basin-scale morphodynamics of the Rhine River. Earth Sci. Rev. 102830.

Gerlach, R., 2003. Historische Auenmorphologie und ihre Nutzung im Duisburger Altstadtgebiet. In: Schirmer, W. (Ed.), Landschaftsgeschichte im europäischen Rheinland. GeoArcheoRhein 4, pp. 461–481.

Gerlach, R., 2006. Holozän: Die Umgestaltung der Landschaft durch den Menschen seit dem Neolithikum. In: Kunow, J., Wegner, H. (Eds.), Urgeschichte im Rheinland. Verlag des Rheinischen Vereins für Denkmalpflege und Landschaftsschutz, Köln, pp. 87–98.

Gouw, M.J.P., Erkens, G., 2007. Architecture of the Holocene Rhine-Meuse delta (the Netherlands) – a result of changing external controls. Neth. J. Geosci. 86, 23–54. https://doi.org/10.1017/S0016774600021302.

Grimm, U., Heinrich, J., 2019. Leipzig 1015 CE – a multiproxy study to reconstruct the palaeorelief of Leipzig's city centre. Archaeol. Prospect. 26, 225–237.

Groenhuijzen, M.R., Verhagen, P., 2017. Comparing network construction techniques in the context of local transport networks in the Dutch part of the Roman limes. J. Archaeol. Sci. Rep. 15, 235–251. https://doi.org/10.1016/j.jasrep.2017.07.024.
Groothedde, M., 2010. De 'nieuwe' IJssel: Wat vertellen de geschreven bronnen en archeologische vondsten? Bijdragen en mededelingen historisch jaarboek voor Gelderland 101, 7–26.
Harnischmacher, S., Zepp, H., 2014. Mining and its impact on the earth surface in the Ruhr district (Germany). Z. Geomorphol. 58, 3–22. https://doi.org/10.1127/0372-8854/2013/S-00131.
Harnischmacher, S., Zepp, H., 2010. Bergbaubedingte Höhenänderungen im Ruhrgebiet – Eine Analyse auf Basis digitalisierter historischer Karten. Zeitschrift für Geodäsie, Geoinformation und Landmanagement 6, 386–397.
Heine, K., Siebertz, H., 1980. Abriß der paläogeographischen Entwicklung des unteren Niederrheingebietes. Arbeiten zur Rheinischen Landeskunde 46, 1–13.
Herget, J., Meurs, H., 2010. Reconstructing peak discharges for historic flood levels in the city of Cologne, Germany. Glob. Planet. Chang. 70, 108–116. https://doi.org/10.1016/j.gloplacha.2009.11.011.
Herget, J., Roggenkamp, T., Krell, M., 2014. Estimation of peak discharges of historical floods. Hydrol. Earth Syst. Sci. 18, 4029–4037. https://doi.org/10.5194/hess-18-4029-2014.
Hesselink, A.W., Stelling, G.S., Kwadijk, J.C., Middelkoop, H., 2003. Inundation of a Dutch river polder, sensitivity analysis of a physically based inundation model using historic data. Water Resour. Res. 39, 1–17. https://doi.org/10.1029/2002WR001334.
Heunks, E., van Hemmen, F., 2016. In het krachtenspel van Mens en Waal. Een biografie van het Lentse land. Archeologische Berichten Nijmegen, Gemeente Nijmegen, p. 224.
Höltken, T., Wagner, G., 2015. Frühmittelalterliche Funde am Fuß des Domes. In: Aufleger, M., Schmidt, C. (Eds.), Archäologie im Rheinland 2014. Wissenschaftlichen Buchgesellschaft, Darmstadt, pp. 162–165.
Hoppe, C., 1970. Die großen Flußverlagerungen des Niederrheins in den letzten zweitausend Jahren und ihre Auswirkungen auf Lage und Entwicklung der Siedlungen. PhD thesis, University of Cologne. pp. 88.
Hudson, P.F., Middelkoop, H., Stouthamer, E., 2008. Flood management along the Lower Mississippi and Rhine Rivers (The Netherlands) and the continuum of geomorphic adjustment. Geomorphology 101, 209–236.
Hutchinson, M.F., 1993. Development of a continent-wide DEM with applications in terrain and climate analysis. In: Goodchild, M.F., Parks, B.O., Steyaert, L.T. (Eds.), Environmental Modeling With GIS, pp. 392–399.
Kalweit, H., Buck, W., Felkel, K., Gerhard, H., van Malde, J., Nippes, K.-R., Ploeger, B., Schmitz, W., 1993. Der Rhein unter der Einwirkung des Menschen – Ausbau, Schiffahrt, Wasserwirtschaft. Internationale Kommission für die Hydrologie des Rheingebietes (CHR/KHR) report I-11, 260.
Kirchner, A., Zielhofer, C., Werther, L., Schneider, M., Linzen, S., Wilken, D., Wunderlich, T., Rabbel, W., Meyer, C., Schmidt, J., Schneider, B., Berg-Hobohm, S., Ettel, P., 2017. A multidisciplinary approach in wetland geoarchaeology: survey of the missing southern canal connection of the Fossa Carolina (SW Germany). Quat. Int. 473, 3–20. https://doi.org/10.1016/j.quaint.2017.12.021.
Kleinhans, M.G., Cohen, K.M., Hoekstra, J., IJmker, J.M., 2011. Evolution of a bifurcation in a meandering river with adjustable channel widths, Rhine delta apex, the Netherlands. Earth Surf. Process. Landf. 36, 2011–2027. https://doi.org/10.1002/esp.2222.
Klostermann, J., 1986. Rheinstromverlagerungen bei Xanten während der letzten 10000 Jahre. Natur am Niederrhein 1, 5–16.
Klostermann, J., 1992. Das Quartär der Niederrheinischen Bucht. Geologisches Landesamt Nordrhein-Westfalen, Krefeld, p. 200.
Koomen, A.J.M., Maas, G.J., 2004. Geomorfologische Kaart Nederland (GKN); Achtergronddocument bij het landsdekkende digitale bestand. Wageningen, Alterra, p. 38.
Koster, K., Stafleu, J., Cohen, K.M., 2017. Generic 3D interpolation of Holocene base-level rise and provision of accommodation space, developed for the Netherlands coastal plain and infilled palaeovalleys. Basin Res. 29, 775–797. https://doi.org/10.1016/j.earscirev.2013.10.014.
Krause, G., 1997. Archaeological evidence of medieval shipping from the Old Town of Duisburg, Lower Rhineland. Travel, Technology and Organization in Medieval Europe. Papers of the Medieval Europe Brugge 1997 conference vol. 8, pp. 101–116.
Krause, G., 1999. Duisburg, Lower Rhineland: the harbour and the topography of the town from the Merovingian period to c. 1600. Maritime Topography and the Medieval Town. Papers of the 5th International Conference on Waterfront Archaeology, pp. 109–118.
Krause, G., 2003. Duisburg and its environs at the confluence of Rhine and Ruhr from the Late Antiquity to the Industrial Age – essential aspects of its development according to archaeological and historical sources. In: Helmig, G., et al. (Eds.), Centre, Region, Periphery. Papers of the Medieval Europe Basel 2002 conference vol. 2, pp. 155–165 (Preprinted Papers. Hertingen 2003).
Lewin, J., Ashworth, P.J., 2014. The negative relief of large river floodplains. Earth Sci. Rev. 129, 1–23. https://doi.org/10.1016/j.earscirev.2013.10.014.
Louwe Kooijmans, L.P., 2007. The Gradual Transition to Farming in the Lower Rhine Basin. Proceedings of the British Academy 144 pp. 287–309.
Makaske, B., Maas, G.J., van Smeerdijk, D.G., 2008. The age and origin of the Gelderse IJssel. Netherlands Journal of Geosciences 87, 323–337. https://doi.org/10.1017/S0016774600023386.
Meurers-Balke, J., Knörzer, K.H., Glasmacher, H.A., Berke, H., Gerlach, R., Tegtmeier, U., 1999. Ein spätmittelalterlicher Brunnen in der Duisburger Niederstrasse. Bonner Jahrbücher 199, 347–396.
Mozzi, P., Ferrarese, F., Zangrando, D., Gamba, M., Vigoni, A., Sainati, C., Fontana, A., Ninfo, A., Piovan, S., Rossato, S., Veronese, F., 2018. The modeling of archaeological and geomorphic surfaces in a multistratified urban site in Padua, Italy. Geoarchaeology 33, 67–84. https://doi.org/10.1002/gea.21641.
Overmars, W., 2020. Een Waal verhaal 1500–1700 Emmerich-Nijmegen. Historisch-morfologische atlas van de Rhein en de Waal. PhD dissertation VU Amsterdam, p. 366.
Pierik, H.J., van Lanen, R.J., 2019. Roman and early-medieval occupation patterns in a delta landscape: the link between settlement elevation and landscape dynamics. Quat. Int. 501, 379–392. https://doi.org/10.1080/17445647.2019.1590248.
Pierik, H.J., Stouthamer, E., Cohen, K.M., 2017. Natural levee evolution in the Rhine–Meuse delta, the Netherlands, during the first millennium CE. Geomorphology 295, 215–234. https://doi.org/10.1016/j.geomorph.2017.07.003.
Pierik, H.J., van der Meulen, B., van Lanen, R., Cohen, K., 2018. Holocene palaeoDEMs for the Rhine valley and delta plain, the Netherlands and Germany. EGU General Assembly Conference Abstracts 20, 8155.
Pröschel, B., Lehmkuhl, F., 2019. Paleotopography and anthropogenic deposition thickness of the city of Aachen, Germany. Journal of Maps 15, 269–277. https://doi.org/10.1080/17445647.2019.1590248.
Reuter, H.I., Nelson, A., Jarvis, A., 2007. An evaluation of void-filling interpolation methods for SRTM data. Int. J. Geogr. Inf. Sci. 21, 983–1008.
Röbke, B.R., Schüttrumpf, H., Vött, A., 2016. Effects of different boundary conditions and palaeotopographies on the onshore response of tsunamis in a numerical model – a case study from western Greece. Cont. Shelf Res. 124, 182–199. https://doi.org/10.1016/j.csr.2016.04.010.
Scheller, H., 1957. Der Rhein bei Duisburg im Mittelalter. In: von Roden, G., Tischler, F. (Eds.), Duisburger Forschungen Band 1. Verlag für Wirtschaft und Kultur Werner Renckhoff KG, Duisburg-Ruhrort, pp. 45–87.
Scheller, H., 1965. Laufänderungen des Rheins bei Neuß. Beiträge zur Rheinkunde 17, 3–11.
Schmidt, J., Werther, L., Zielhofer, C., 2018. Shaping pre-modern digital terrain models: the former topography at Charlemagne's canal construction site. PLoS One 13, e0200167. https://doi.org/10.1371/journal.pone.0200167.
Schneider, J., 1886. Die alten Heer- und Handelswege der Germanen, Römer und Franken im deutschen Reiche; Fünftes Heft. T. O. Weigel, Leipzig, p. 23.
Schneider, A., Hirsch, F., Wechler, K.-P., Raab, A., Raab, T., 2017. Reconstruction of a palaeosurface and archaeological site location in an anthropogenic drift sand area. Archaeol. Prospect. 24, 297–310. https://doi.org/10.1002/arp.1571.
Shala, B., 2001. Jungquartäre Talgeschichte des Rheins zwischen Krefeld und Dinslaken. PhD thesis, Düsseldorf. pp. 231.
Stouthamer, E., Cohen, K.M., Gouw, M.J., 2011. Avulsion and its implications for fluvial-deltaic architecture: Insights from the Holocene Rhine-Meuse delta. SEPM Spec. Publ. 97, 215–232.
Straßer, R., 1989. Geschichtlicher Atlas der Rheinlande Beiheft I/6. Veränderungen des Rheinlaufs zwischen Wupper- und Düsselmündung seit der Römerzeit. Gesellschaft für Rheinische Geschichtskunde, Köln, p. 38.
Tarolli, P., Sofia, G., 2016. Human topographic signatures and derived geomorphic processes across landscapes. Geomorphology 255, 140–161. https://doi.org/10.1016/j.geomorph.2015.12.007.
Toonen, W.H., 2013. A Holocene Flood Record of the Lower Rhine. PhD thesis, Utrecht. pp. 204.
Toonen, W.H., de Molenaar, M.M., Bunnik, F.P., Middelkoop, H., 2013. Middle Holocene palaeoflood extremes of the Lower Rhine. Hydrol. Res. 44, 248–263. https://doi.org/10.2166/nh.2012.162.
van de Ven, G.P., 1976. Aan de wieg van Rijkswaterstaat: wordingsgeschiedenis van het Pannerdens Kanaal. De Walburg Pers, Zutphen, p. 438.
van der Meulen, B., Deggeller, T.S., Bomers, A., Cohen, K.M., Middelkoop, M., 2018. The historical river: morphology of the Rhine before river normalization. In: Huismans, Y., Berends, K.D., Niesten, I., Mosselman, E. (Eds.), The Future River: NCR Days 2018 Proceedings. Netherlands Centre for River Studies Publication 42-2018, pp. 44–45.
van Lanen, R.J., Pierik, H.J., 2019. Calculating connectivity patterns in delta landscapes: modelling Roman and early-medieval route networks and their stability in dynamic lowlands. Quat. Int. 501, 393–412. https://doi.org/10.1016/j.quaint.2017.03.009.
van Lanen, R.J., Jansma, E., van Doesburg, J., Groenewoudt, B.J., 2016. Roman and early-medieval long-distance transport routes in north-western Europe: modelling frequent-travel zones using a dendroarchaeological approach. J. Archaeol. Sci. 73, 120–137.
van Lanen, R.J., de Kleijn, M.T.M., Gouw-Bouman, M.T.I.J., Pierik, H.J., 2018. Exploring Roman and early-medieval habitation of the Rhine–Meuse delta: modelling large-scale demographic changes and corresponding land-use impact. Neth. J. Geosci. 97, 45–68. https://doi.org/10.1017/njg.2018.3.
Verhagen, J., Kluiving, S.J., Anker, E., van Leeuwen, L., Prins, M.A., 2017. Geoarchaeological research for Roman waterworks near the late Holocene Rhine-Waal delta bifurcation, the Netherlands. Catena 149, 460–473. https://doi.org/10.1016/j.catena.2016.03.027.
Vermeer, J.A.M., Finke, P.A., Zwertvaegher, A., Gelorini, V., Bats, M., Antrop, M., Verniers, J., Crombé, P., 2014. Reconstructing a prehistoric topography using legacy point data in a depositional environment. Earth Surf. Process. Landf. 39, 632–645. https://doi.org/10.1016/j.eswa.2010.12.162.
Werbrouck, I., Antrop, M., van Eetvelde, V., Stal, C., de Maeyer, P., Bats, M., Bourgeois, J., Court-Picon, M., Crombé, P., de Reu, J., de Smedt, P., Finke, P.A., van Meirvenne, M., Verniers, J., Zwertvaegher, A., 2011. Digital Elevation Model generation for historical landscape analysis based on LiDAR data, a case study in Flanders (Belgium). Expert Syst. Appl. 38, 8178–8185. https://doi.org/10.1016/j.eswa.2010.12.162.
Willemse, N.W., 2019. De vroege Waal bij Nijmegen. Stratigrafie, sedimentologie en genese van laat holocene rivierafzettingen tussen Nijmegen en Lent. Gemeente Nijmegen, Plangebied 'Ruimte voor de Waal'. RAAP Rapport 3208. p. 335.
Wronna, M., Baptista, M.A., Götz, J., 2017. On the construction and use of a paleo-DEM to reproduce tsunami inundation in a historical urban environment – the case of the 1755 Lisbon tsunami in Cascais. Geomatics, Natural Hazards and Risk 8, 841–862. https://doi.org/10.1080/19475705.2016.1271832.
Zhou, D., 2000. Jungquartäre Talgeschichte des mittleren Niederrheins. PhD thesis, Düsseldorf. pp. 249.